



Supplement of

Comparison of particle number size distribution trends in ground measurements and climate models

Ville Leinonen et al.

Correspondence to: Annele Virtanen (annele.virtanen@uef.fi) and Ville Leinonen (ville.j.leinonen@uef.fi)

The copyright of individual parts of the supplement might differ from the article licence.

S1 Seasonality, SeasC and NIQR

Seasonality of measured and modelled N were compared using SeasC for maximum seasonal variation and NIQR for average seasonal variation. In this seasonal comparison, we have concentrated on Aitken and accumulation modes. The results for the nucleation mode are shown in Fig. S18 for maximum variation and in Fig. S21 for average variation. In Figures S19 and S20, maximum variations are shown for Aitken and accumulation mode, respectively. The figures also indicate during which season the minimum and maximum values usually occur.

The maximum variation of medians of measured data values were mostly insensitive to the representation of the data, especially for the accumulation mode, although interquartile ranges did show some variation with varying measurement data representation. Notable exceptions to this general statement were the Aitken mode SeasC values for Zeppelin, K-Pusztá, and San Pietro Capofiume. The strong dependence of the Aitken mode SeasC on data representation at Zeppelin is most likely due to the very clean conditions there, which easily leads to large variations in relative changes. At K-Pusztá and San Pietro Capofiume, the results from measurement representations appeared to be very sensitive to the assumed upper bound of the Aitken mode, which is 50 nm for the sectional representation and 100 nm for the modal representation. This could result in a shift of particle number between Aitken and accumulation modes and hence could affect the computed SeasC value, especially if the effect was different for different seasons. This becomes apparent when comparing Figs. S19 and S20, where for these two sites the sectional representation had a larger Aitken mode SeasC and a smaller accumulation mode SeasC. The season during which the minimum and maximum values in N occur were also mostly independent of data representation, but in some cases shifted to an earlier or later season.

For maximum variation (SeasC) in measured data, there was a clear difference between remote and more polluted sites, with seasonal variations in N s being higher in remote sites. Remote sites had generally larger maximum variation due to the more dominating effect of naturally emitted (organic) particles and particle precursors during summer, which was affecting especially the Aitken mode maximum N and, hence increasing maximum variation. For measured maximum variation, three sites, Zeppelin (polar), Pallas (remote), and Värriö (remote) had the highest maximum variation, meaning that N in summer could be 3-10 times higher than concentrations in winter. For urban and other polluted sites, seasonal variation was much smaller, having maximum variation values of less than 2. Results for measured maximum variation with respect to site classes were consistent with findings of Rose et al. (2021), who presented SeasC results for total N s measured in 62 sites globally in 2016 or 2017.

ECHAM-SALSA, NorESM1.2, and UKESM1 had larger maximum variation for polar and remote sites than for urban sites, which was also observed in measurements. However, sometimes the maximum variation was overestimated. ECHAM-SALSA and NorESM1.2 especially seemed to overestimate the Aitken mode maximum variation in many of the sites investigated in this study. For northern sites, Pallas, Värriö, and Zeppelin, higher maximum variation in models was not the only difference, but also the seasonal cycle in these two models was similar to the measured, but different compared to the other three models, as seen for example for Aitken mode in Fig. 14. In addition, compared to the observed modes in Hyytiälä, Melpitz, K-Pusztá, Vavihill, Puijo, and Helsinki, NorESM1.2 and ECHAM-SALSA had lower N s especially during winter, and this results in higher annual variation.

In Figures S22 and S23, measured average seasonal variation in Aitken and accumulation mode N was investigated with NIQR. NIQR had similar patterns as SeasC. This was expected, as both quantities measure seasonal variation, with SeasC focusing more on extreme values. For Aitken mode, the largest average variations were seen in remote sites Zeppelin, Pallas, and Värriö. For accumulation mode, the differences were smaller, remote sites having the largest values, which

were smaller than for Aitken mode. In addition, models seemed to mostly capture average seasonal variation similarly as they captured maximum variation in Aitken and accumulation mode.

In general, models captured average seasonal variation (NIQR) slightly better than maximum variations (SeasC). Variability in the interquartile range was, therefore, better accounted for than the seasonal extremes, which were resulting in higher modelled maximum variation than observations. The reason for higher maximum variation is diverse: for Aitken mode, it is usually due to underestimated lowest interquartile range and especially too small concentrations observed during winter months, whereas for accumulation mode, higher modelled concentrations during summer were usually causing too high maximum variation in models. However, in the big picture, the seasonality variables (NIQR and SeasC) got larger values in remote areas and smaller values in more polluted areas, which was seen in the models even though the magnitude of the seasonality was overestimated or underestimated.

For measured seasonal extremes in the Aitken mode, almost all sites had their minimum concentrations in winter or autumn. Only San Pietro Capofiume had its minimum in Spring. At the other sites, maxima in Aitken mode were either in summer or spring. The seasonal pattern for Aitken mode concentrations was not similar in models compared to measurements, where NorESM1.2 seemed to capture seasonal extremes best, except the magnitude of extremes, which was sometimes overestimated. Aitken mode minimum was more often captured by the models than maximum.

For Accumulation mode, measurements did not show clear differences in average seasonal variation and maximum variation of number concentration between remote and other sites, despite measured maximum variation had on average been slightly larger for remote sites. However, maximum variation of accumulation mode N was smaller than maximum variation of Aitken mode in remote sites. Especially NorESM1.2 and also ECHAM-SALSA seemed to overestimate the maximum variation of the Accumulation mode N in most of the sites. These overestimates were in almost all cases due to higher modelled N s in summer compared to what has been observed.

For seasonal extremes in the accumulation mode, most of the sites had their (observational) minimum concentration either in winter or autumn and maximum in spring or summer. Exceptions were San Pietro Capofiume where the minimum was during spring and maximum in winter, Mace Head where minimum was during summer and maximum during spring, and K-Pusztá where the minimum was during summer and maximum in winter. Summer maxima were mostly captured by the models, and in general better than for Aitken mode. For the accumulation mode, the season of maximum number concentration was better captured by the models than the minimum.

The annual cycles of N s varied between models, modes, and sites. When calculating the total number of seasonal extremes captured by the models, NorESM1.2 captured most of the seasonal extremes in nucleation, Aitken, and accumulation mode for all sites (33 correct seasons/78 = 6 extremes * 13 sites), followed by ECHAM-M7 (31), ECHAM-SALSA (29), UKESM (26) and EC-Earth (22) when model extremes were compared to mode fitting results. Results were varying between different modes, ECHAM-M7 and ECHAM-SALSA had best captured the nucleation mode extremes. NorESM1.2 was best for Aitken mode and UKESM1 showed the best results for accumulation mode.

S2 Additional figures

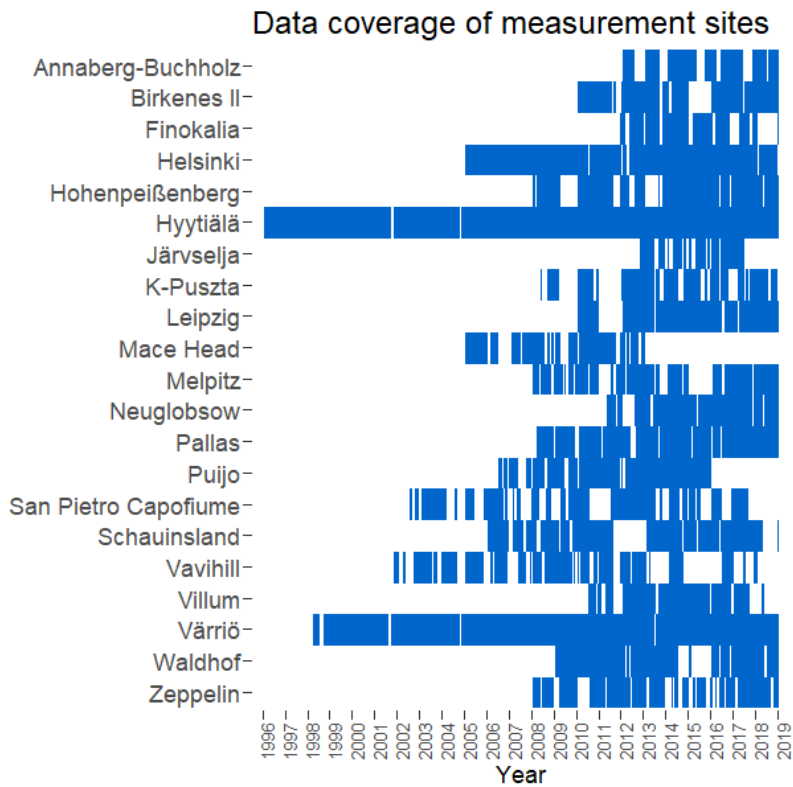


Figure S1 Data coverage of measurement sites. Blue represents the periods where daily averaged data have been calculated, i.e., there is at least 5 measurement points/day. The data coverage of the sites is between 59.6 and 98.4% of the days in the measured period.

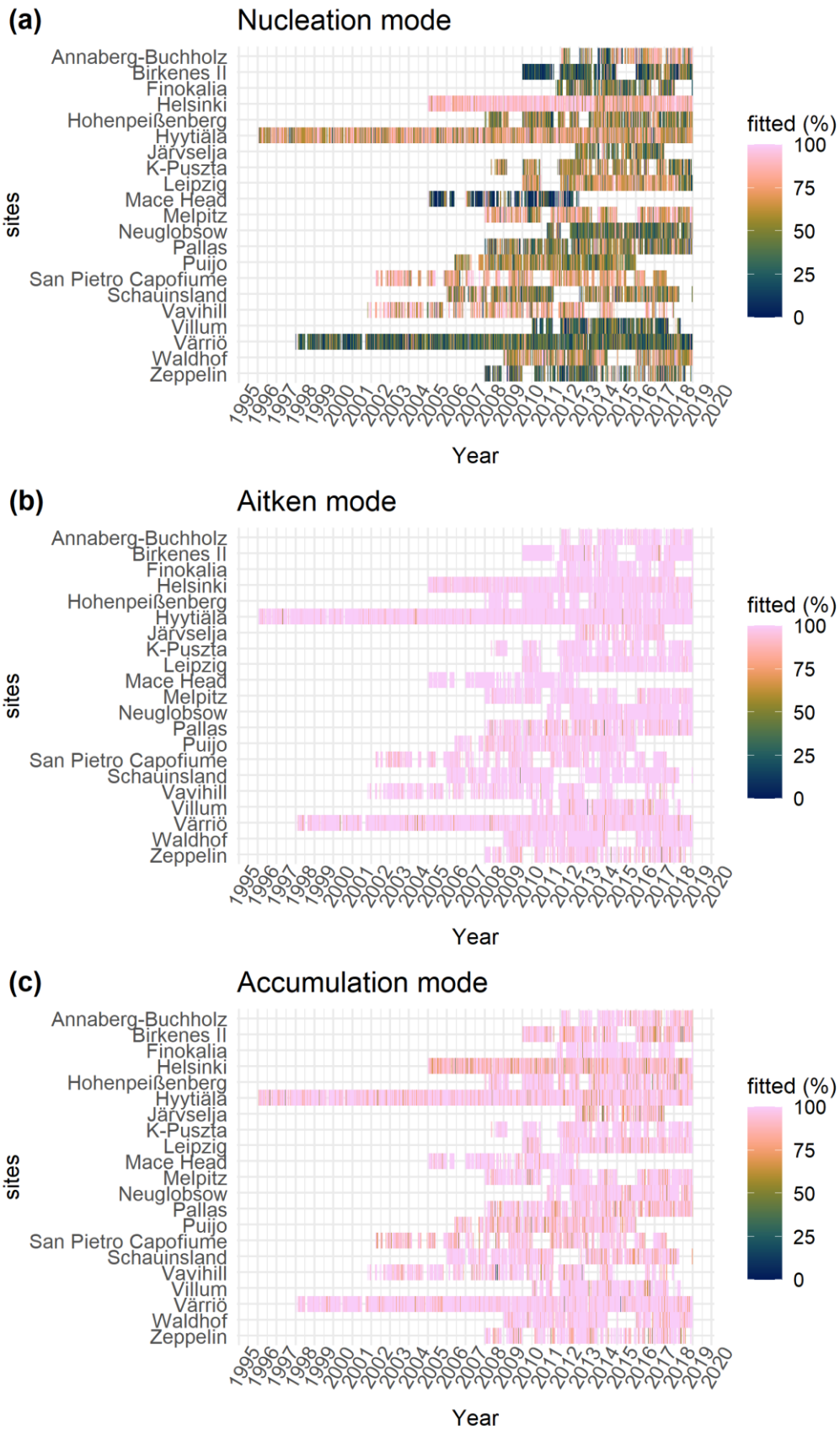


Figure S2 Percentages of fitted nucleation (a), Aitken (b), and accumulation (c) modes at each day and at different sites during the whole measurement time series.

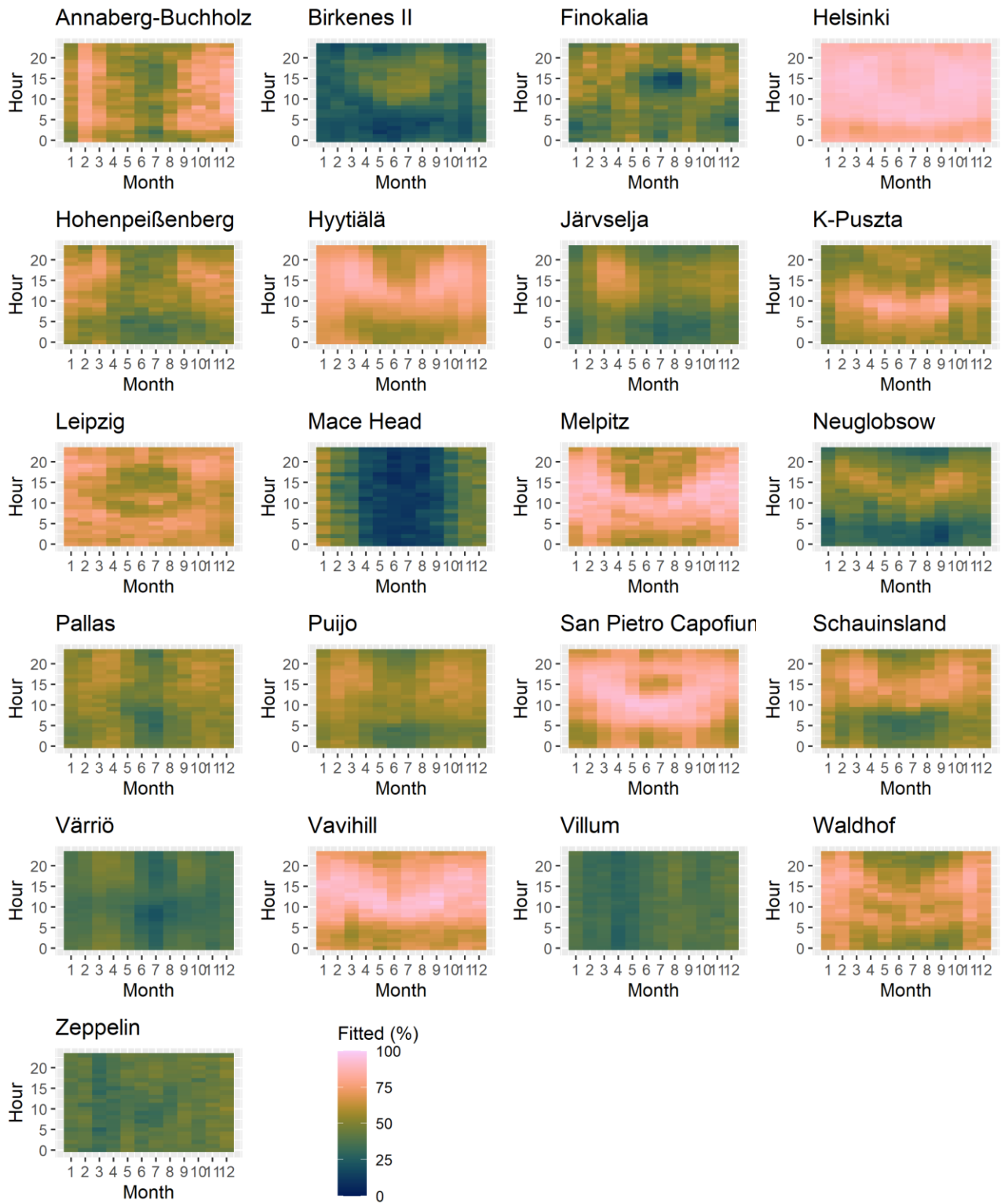


Figure S3 Mean percentages of fitted nucleation modes at each hour and month at different sites during the whole measurement time series.

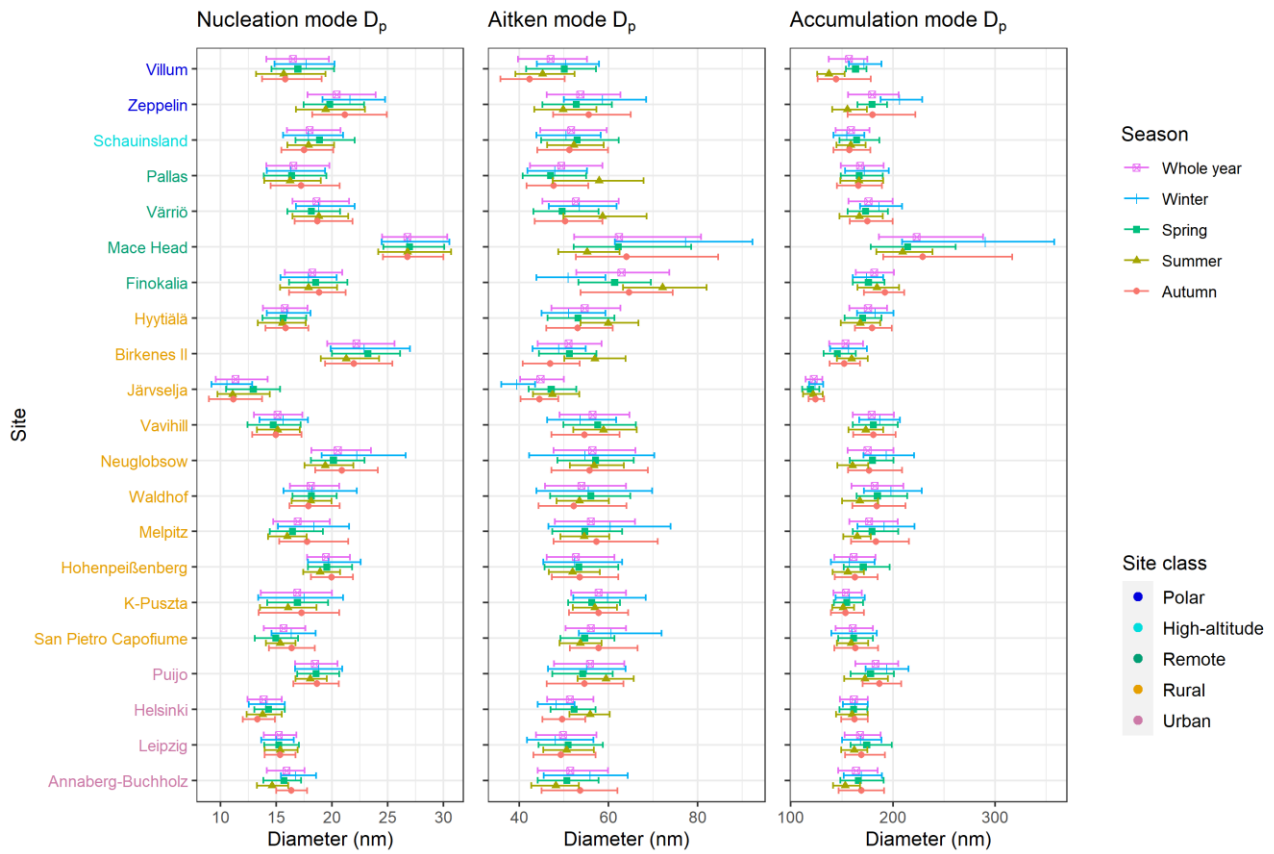


Figure S4 Summary of geometric nucleation, Aitken, and accumulation mode mean diameter D_p for measurement sites and different seasons (winter = Dec, Jan, Feb, spring = Mar, Apr, May, summer = Jun, Jul, Aug, autumn = Sep, Oct, Nov). Medians (dots) and interquartile ranges (25% and 75%, whiskers) for different mode parameters in fitted modes.

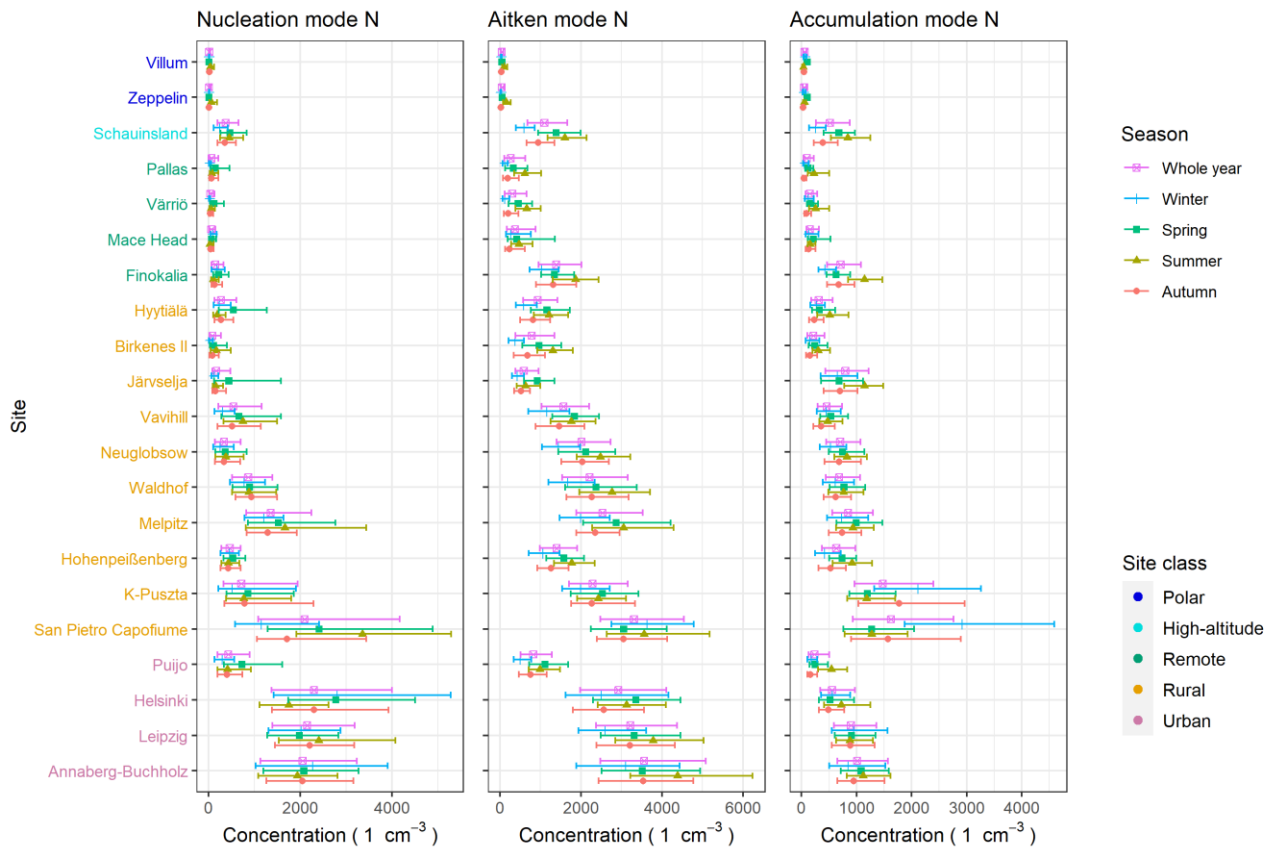


Figure S5 Summary of nucleation, Aitken, and accumulation mode number concentration (N) for measurement sites and different seasons (winter = Dec, Jan, Feb, spring = Mar, Apr, May, summer = Jun, Jul, Aug, autumn = Sep, Oct, Nov). Medians (dots) and interquartile ranges (25% and 75%, whiskers) for different mode parameters in fitted modes.

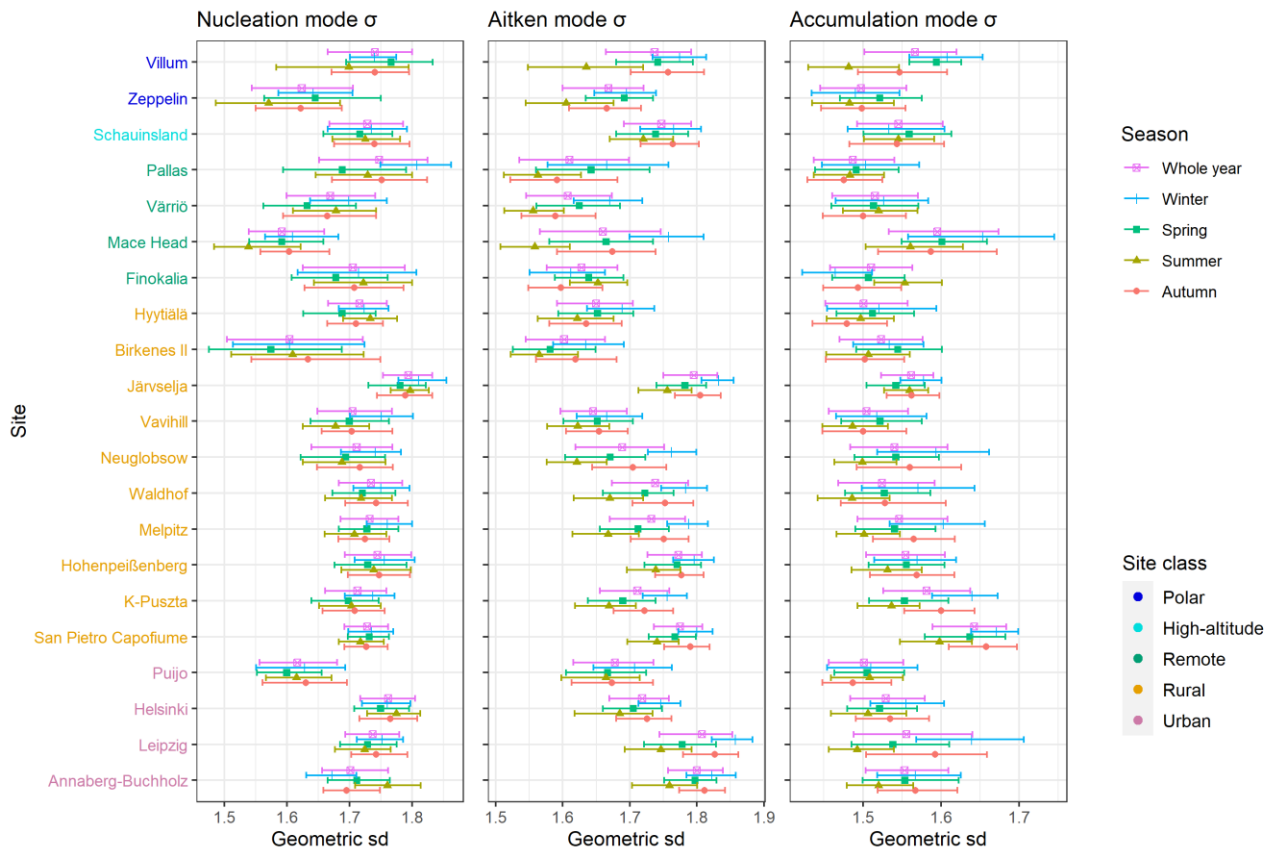


Figure S6 Summary of nucleation, Aitken, and accumulation mode geometric standard deviation σ for measurement sites and different seasons (winter = Dec, Jan, Feb, spring = Mar, Apr, May, summer = Jun, Jul, Aug, autumn = Sep, Oct, Nov). Medians (dots) and interquartile ranges (25% and 75%, whiskers) for different mode parameters in fitted modes.

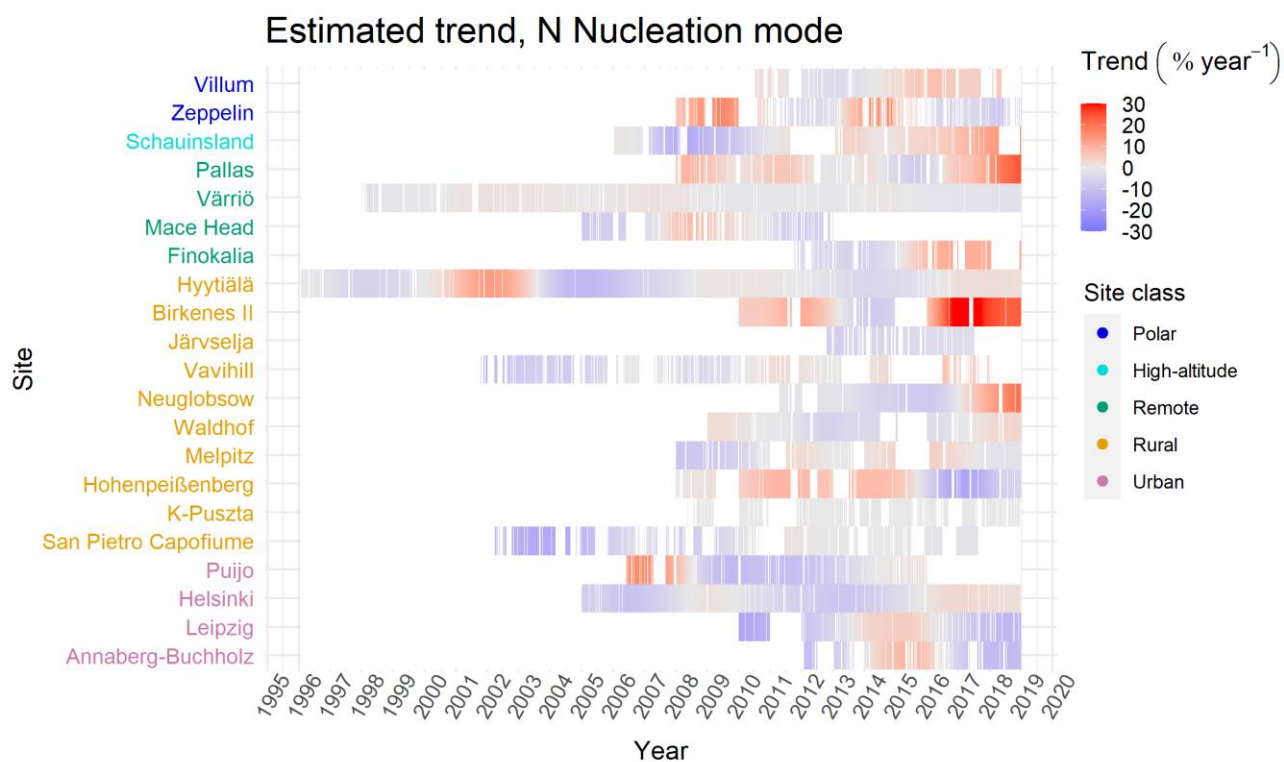
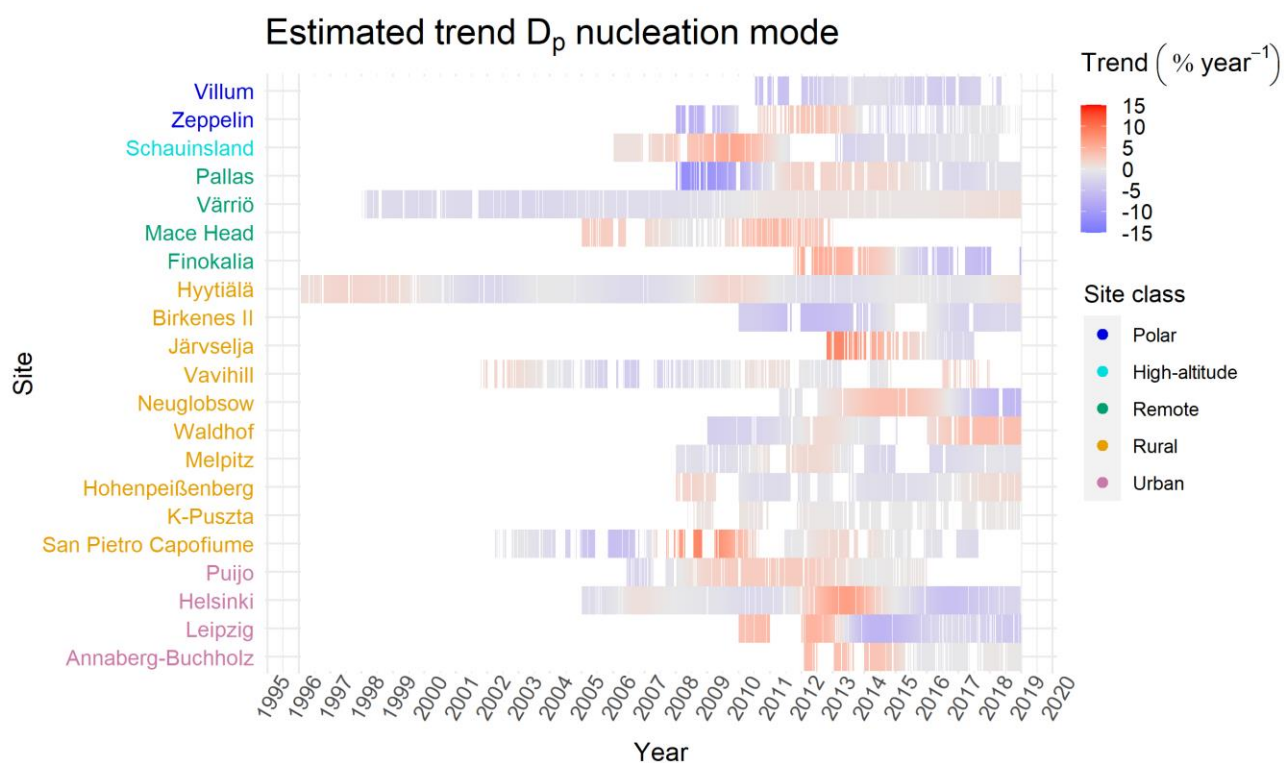


Figure S7 Estimated trends for nucleation mode D_p and N at measurement sites. Trend has been calculated by DLM, see section 2.3.1 for details. The overall trend presented in the figure is comparable with the long-term trend estimates given in section 3.1. To get a DLM trend for one year, the one-day trend given by the model was multiplied by the number of days in a year (365 used for all years) and divided by the mean of the variable over the first observed year. For example, if the trend is showing an increase of 10% / year it means that if the short-term increase would continue for a year, the concentration would be increased by 10% during the year compared to the first year mean.

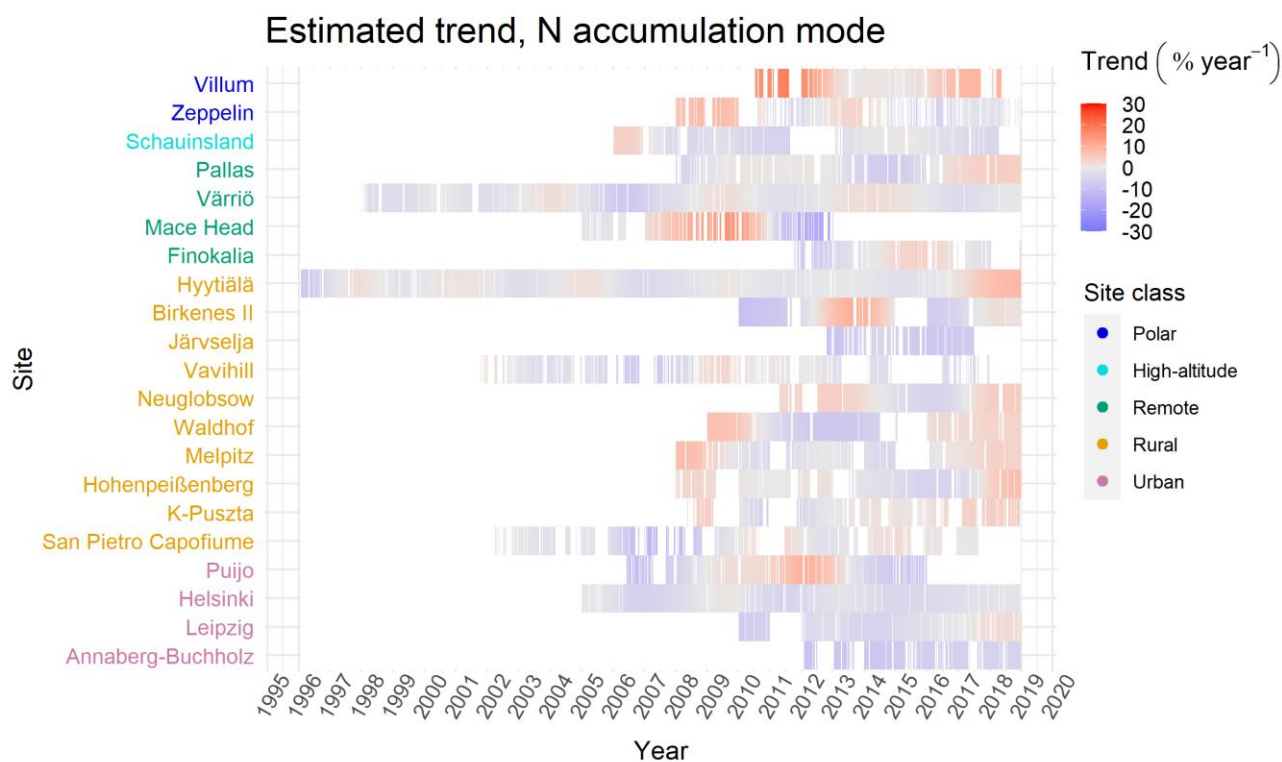
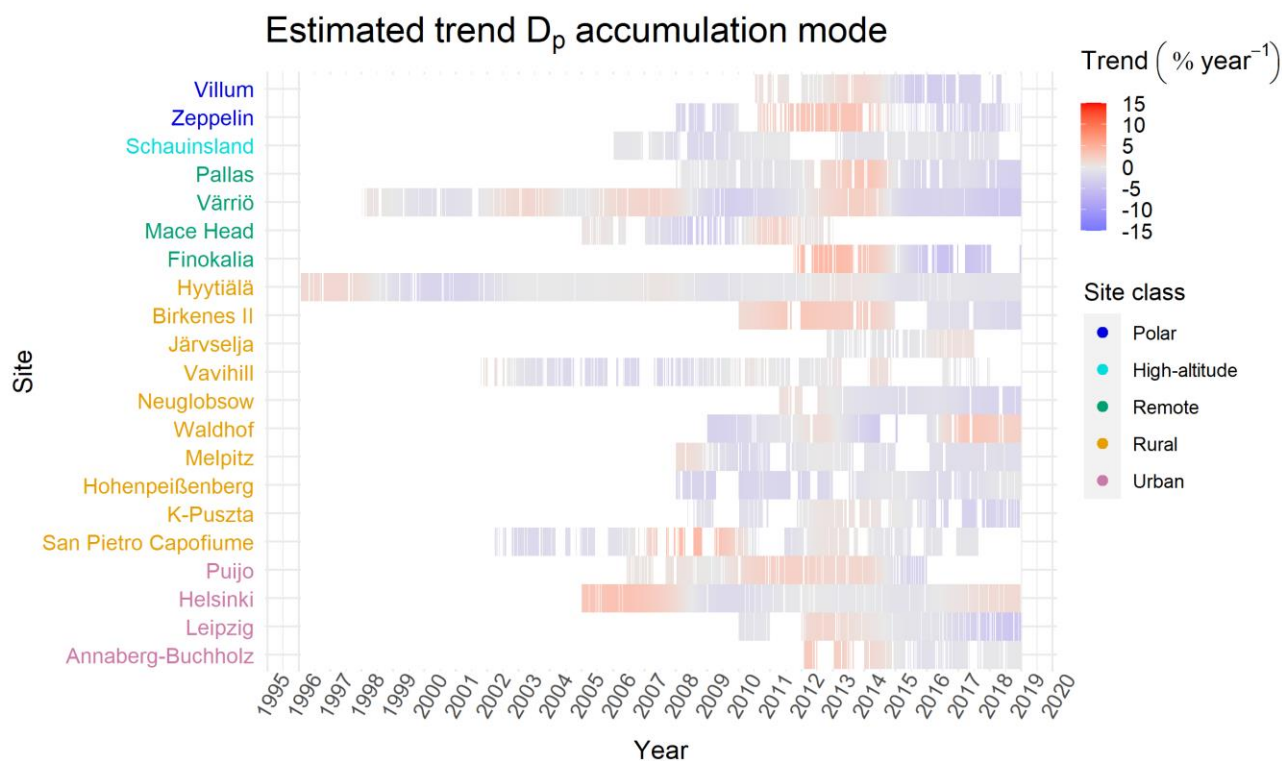
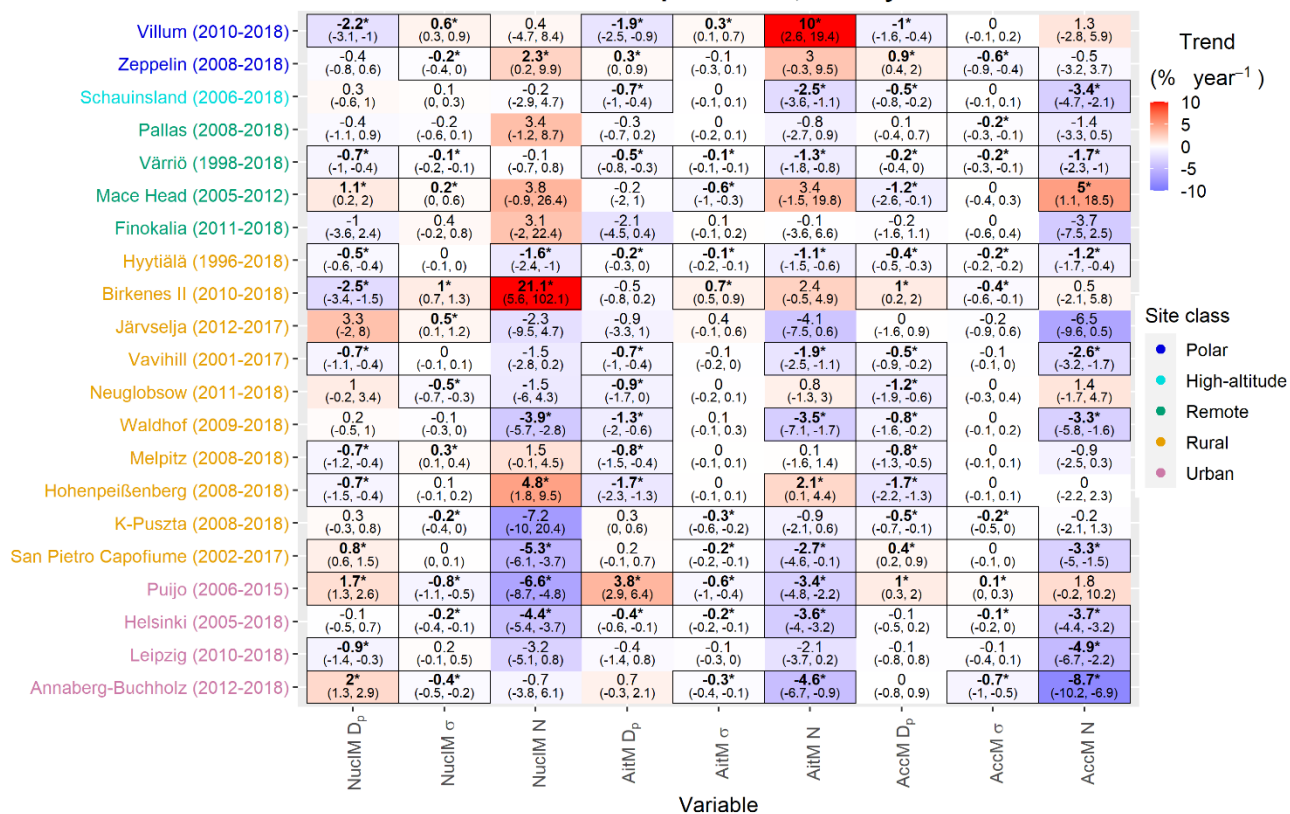


Figure S8 Estimated trends for accumulation mode D_p and N at measurement sites. Trend has been calculated by DLM, see section 2.3.1 for details. The overall trend presented in the figure is comparable with the long-term trend estimates given in section 3.1. To get a DLM trend for one year, the one-day trend given by the model was multiplied by the number of days in a year (365 used for all years) and divided by the mean of the variable over the first observed year. For example, if the trend is showing an increase of 10% / year it means that if the short-term increase would continue for a year, the concentration would be increased by 10% during the year compared to the first year mean.

Sen-Theil estimators for mode parameters, whole year data



Trend
(% year⁻¹)

Site class

- Polar
- High-altitude
- Remote
- Rural
- Urban

Figure S9 Long-term trend estimators for measured trends of all mode parameters (mean geometric diameter D_p , geometric standard deviation σ , and number concentration N) in nucleation (NuclM), Aitken (AitM), and accumulation mode (AccM). Statistically significant (95% confidence level) trends are bolded, marked with an asterisk, and highlighted with border lines. Trends have been calculated using Sen-Theil estimator and complemented with bootstrap confidence intervals (see section 2.3.2).

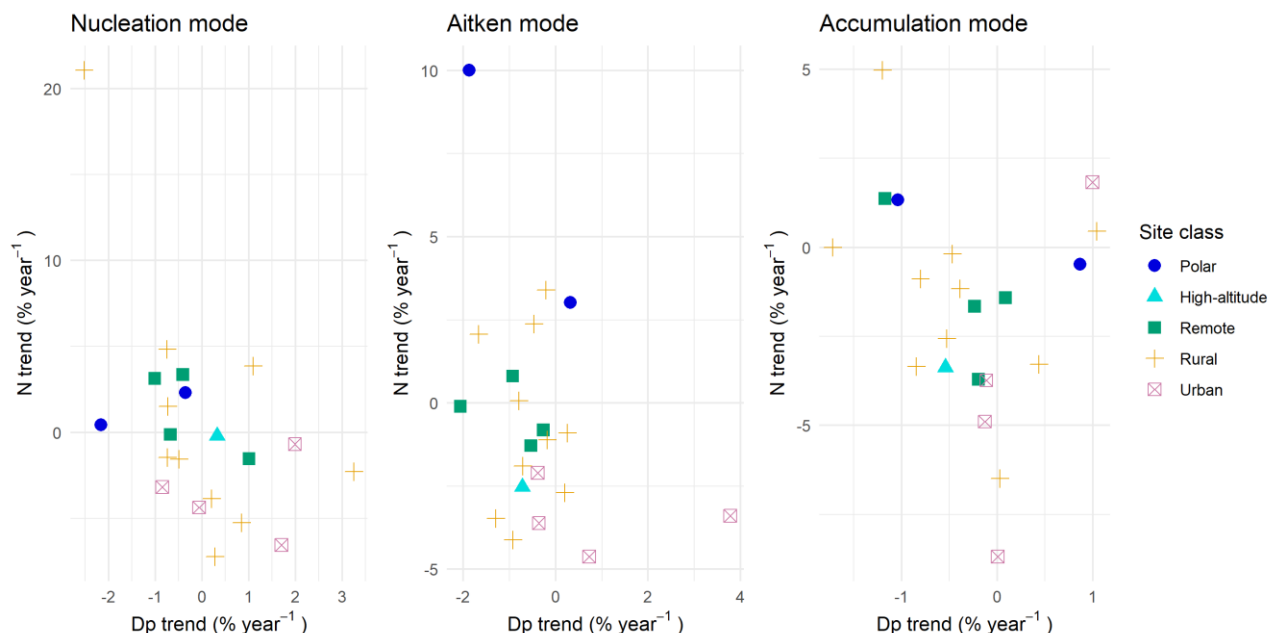
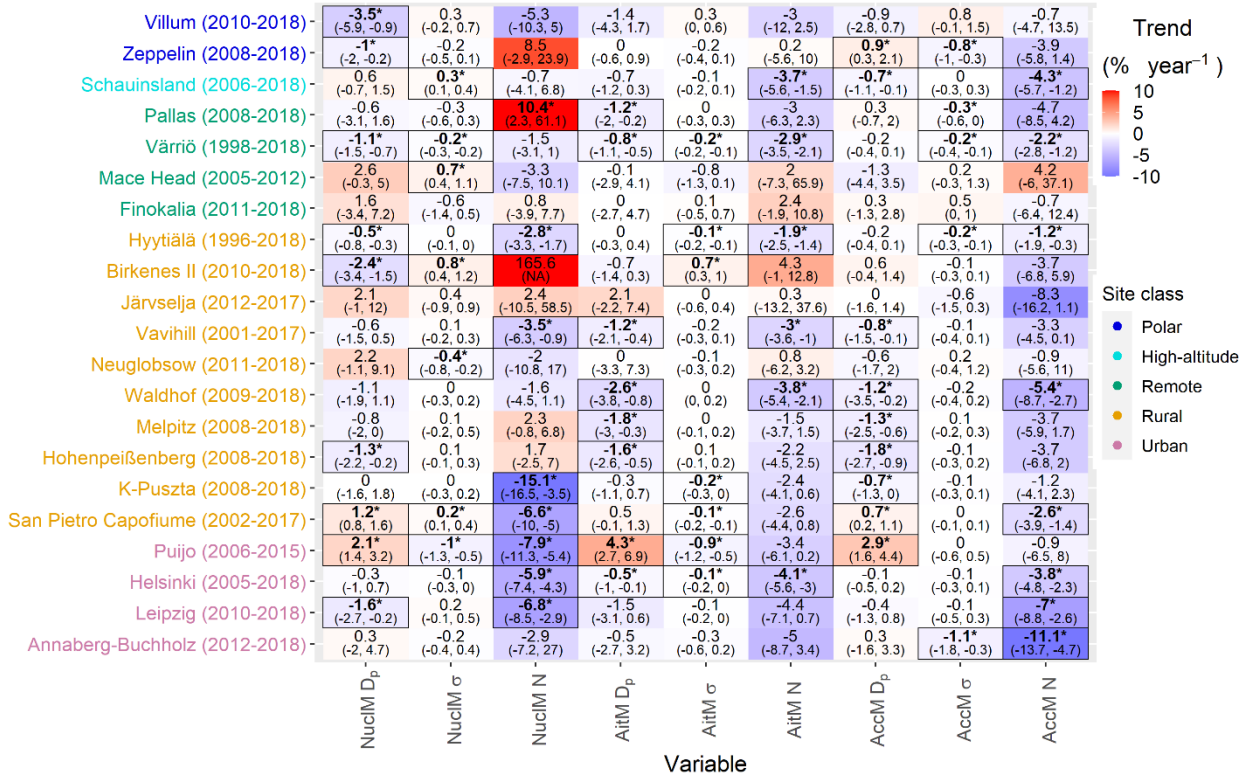


Figure S10 Scatter plot of mean geometric diameter D_p and number concentration N trends for nucleation, Aitken, and accumulation mode (trends are shown also in Fig. S9). Colour of the dots represent the site classification of each site (see Table 1 for environmental site classification).

Sen-Theil estimators for mode parameters, Winter



Sen-Theil estimators for mode parameters, Summer

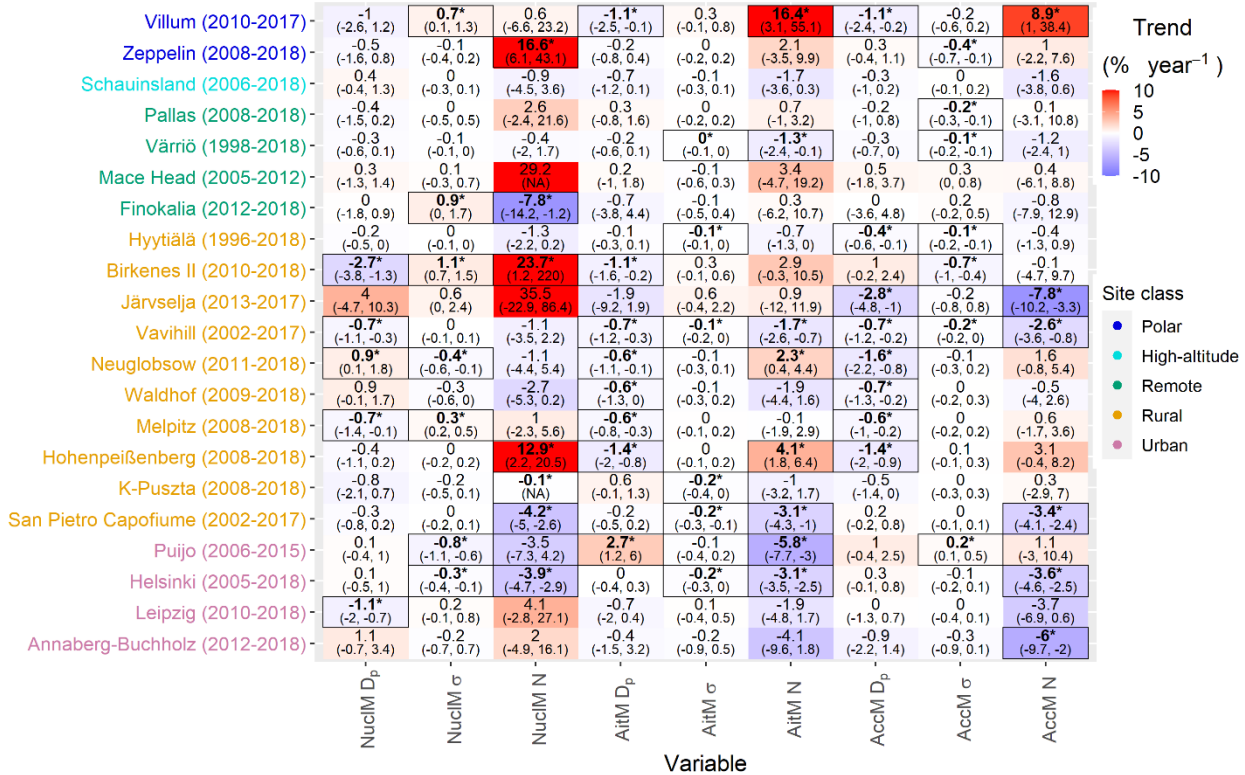
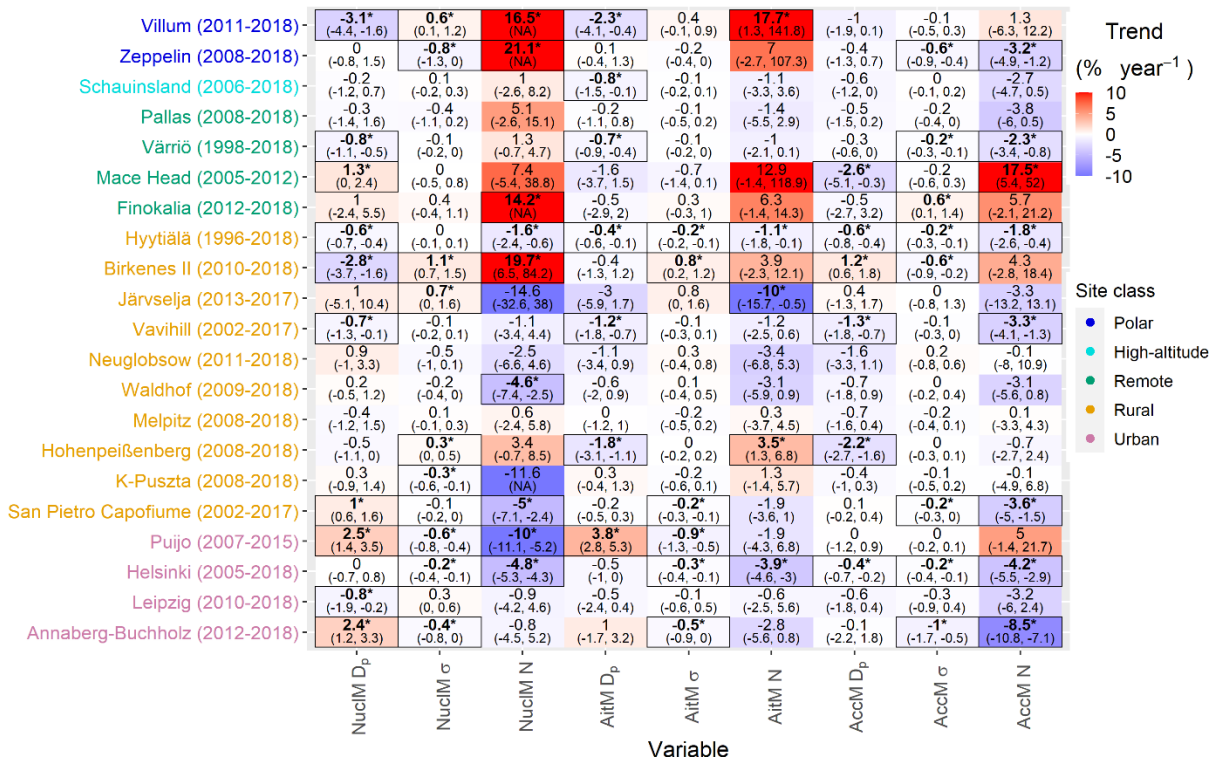


Figure S11 Seasonal long-term trend estimates for all mode parameters (mean geometric diameter D_p , geometric standard deviation σ , and number concentration N in nucleation (NuclM), Aitken (AitM), and accumulation mode (AccM) during winter (January, February, and December) and summer (June, July, and August). Statistically significant (95% confidence level) trends are bolded, marked with an asterisk, and highlighted with border lines. Trends have been calculated using Sen-Theil estimator and complemented with bootstrap confidence intervals (see section 2.3.2). For some cases, function was not able to calculate confidence interval correctly, we have marked those intervals with “(NA)”.

Sen-Theil estimators for mode parameters, Spring



Sen-Theil estimators for mode parameters, Autumn

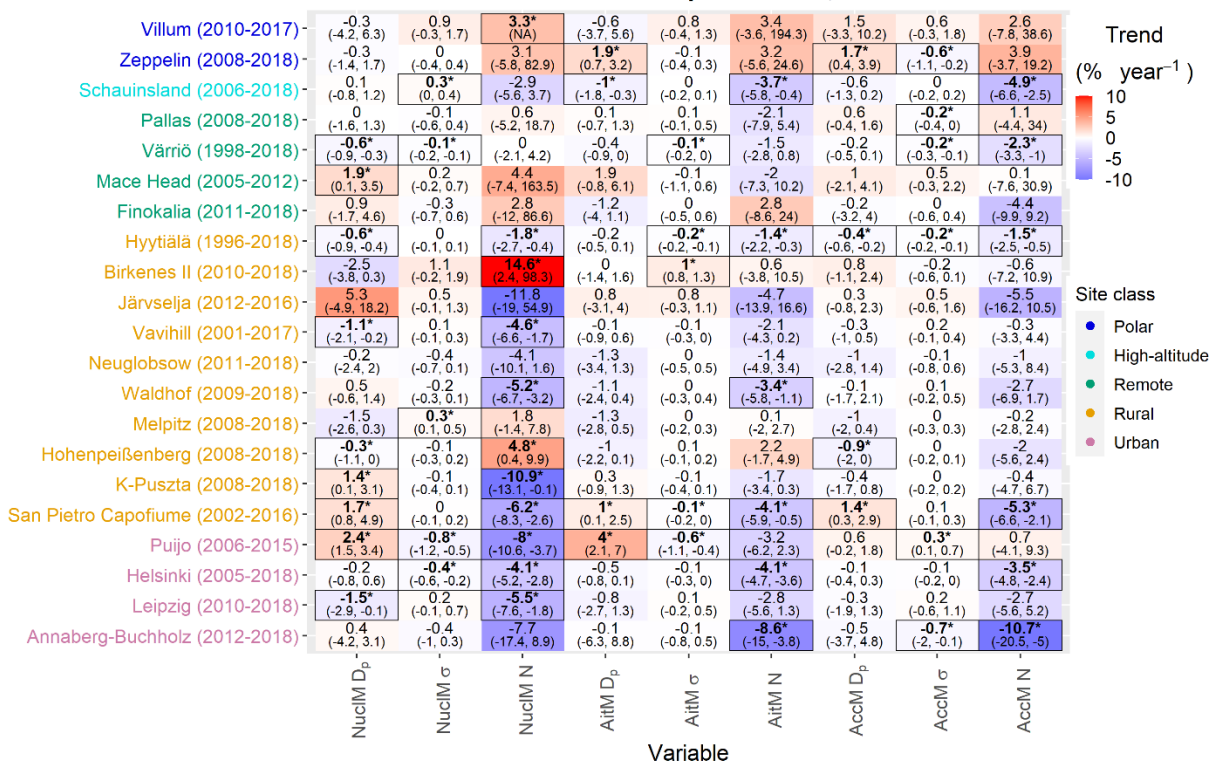
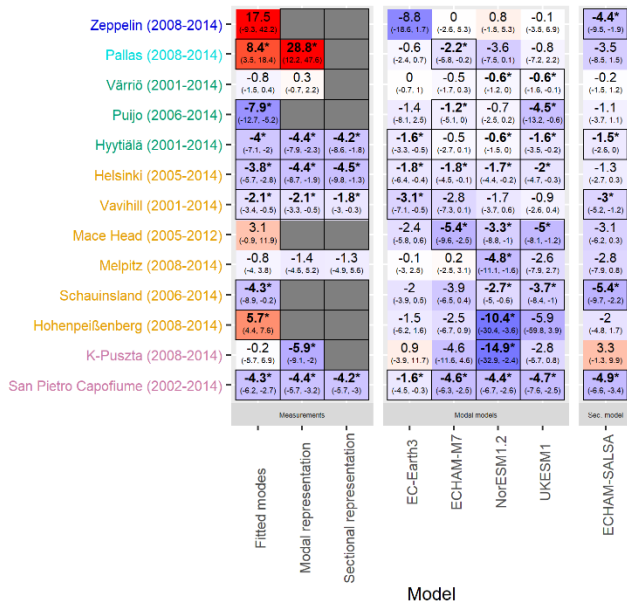
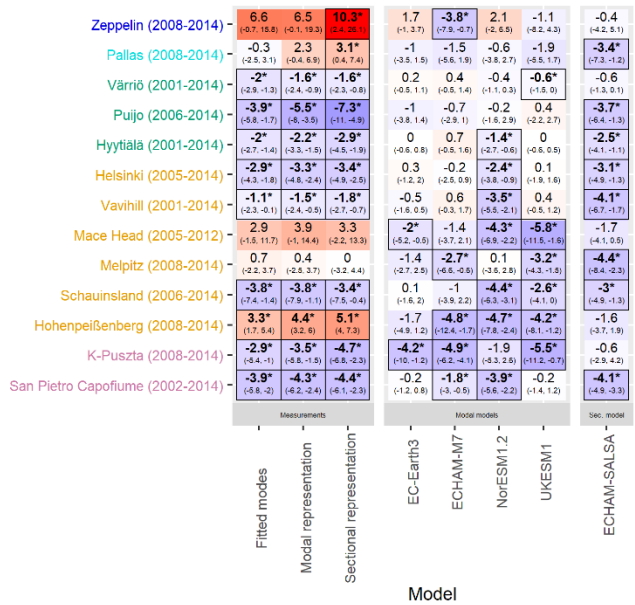


Figure S12 Seasonal long-term trend estimates for all mode parameters (mean geometric diameter D_p , geometric standard deviation σ , and number concentration N in nucleation (NuclM), Aitken (AitM), and accumulation mode (AccM) during spring (March, April, and May) and autumn (September, October, and November). Statistically significant (95% confidence level) trends are bolded, marked with an asterisk, and highlighted with border lines. Trends have been calculated using Sen-Theil estimator and complemented with bootstrap confidence intervals (see section 2.3.2). For some cases, function was not able to calculate confidence interval correctly, we have marked those intervals with “(NA)”.

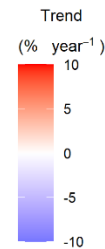
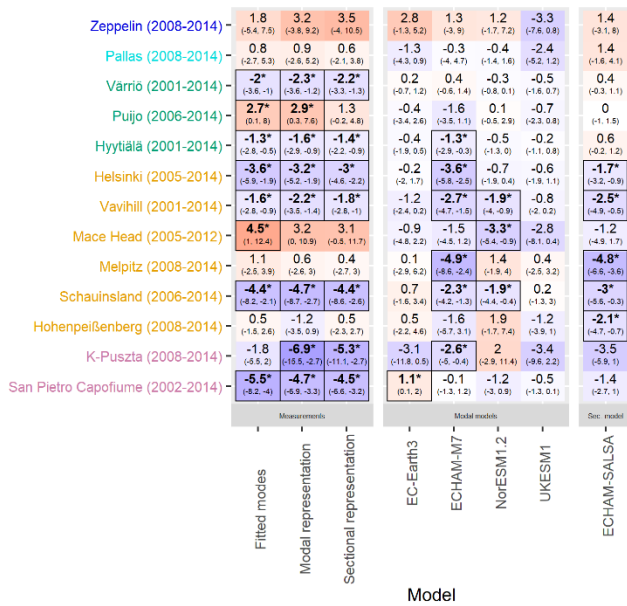
Long-term trends for Nucleation mode



Long-term trends for Aitken mode



Long-term trends for accumulation mode



Site class

- Polar
- High-altitude
- Remote
- Rural
- Urban

Figure S13 Long-term trend estimates for measured and modelled nucleation, Aitken, and accumulation mode number concentration. The sites (y axis) are arranged by site class and within site class most northerly to most southerly. Statistically significant (95% confidence level) trends are bolded, marked with an asterisk, and surrounded by a black border.

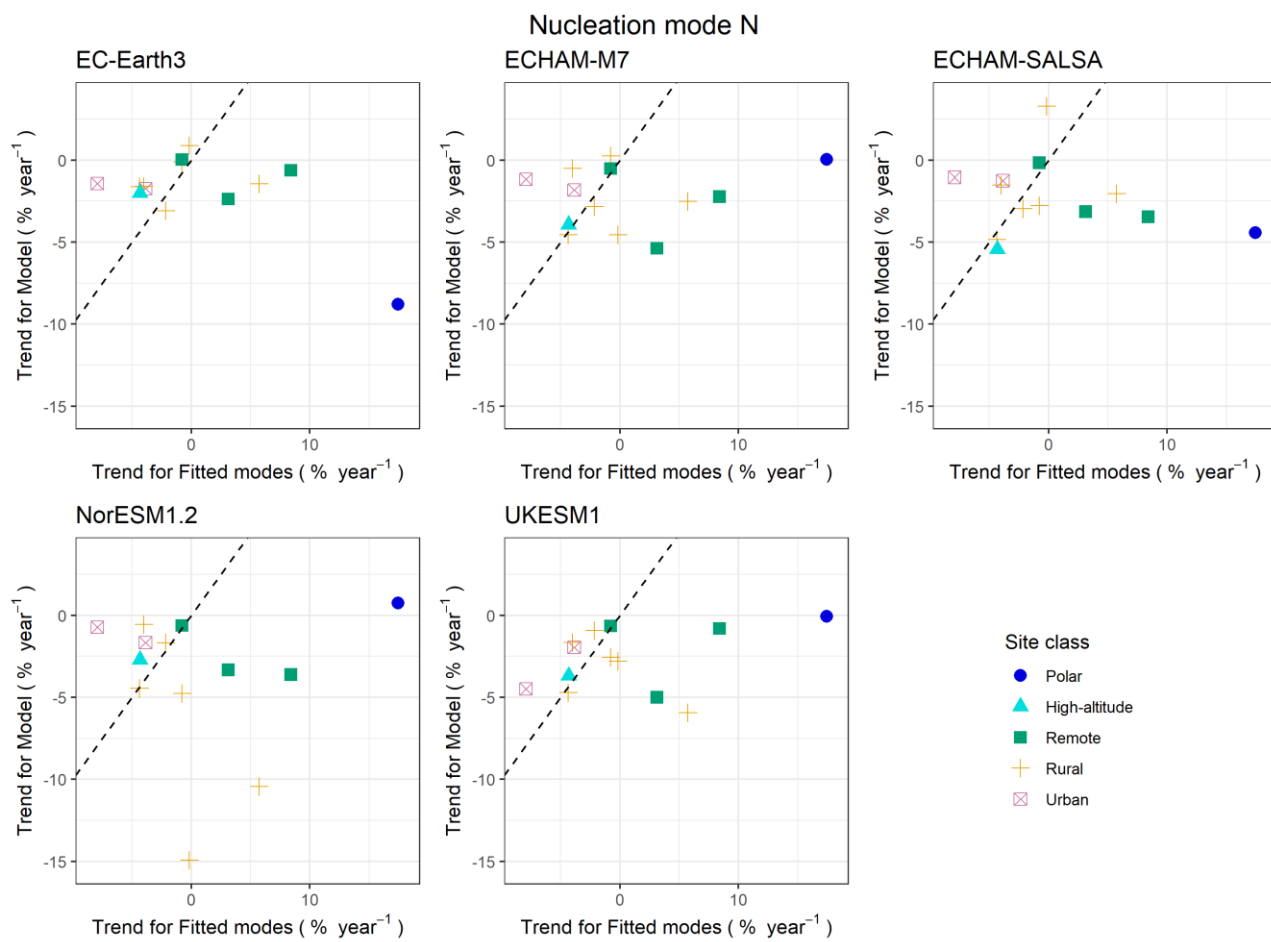


Figure S14 Scatter plots of number concentration (N) long-term trend estimates of measurements (Fitted mode) and climate models (model as a subplot title) for nucleation mode based on the data used for model comparison. Colour and shape of dots represent the site classification of each site (see Table 1 for environmental site classification).

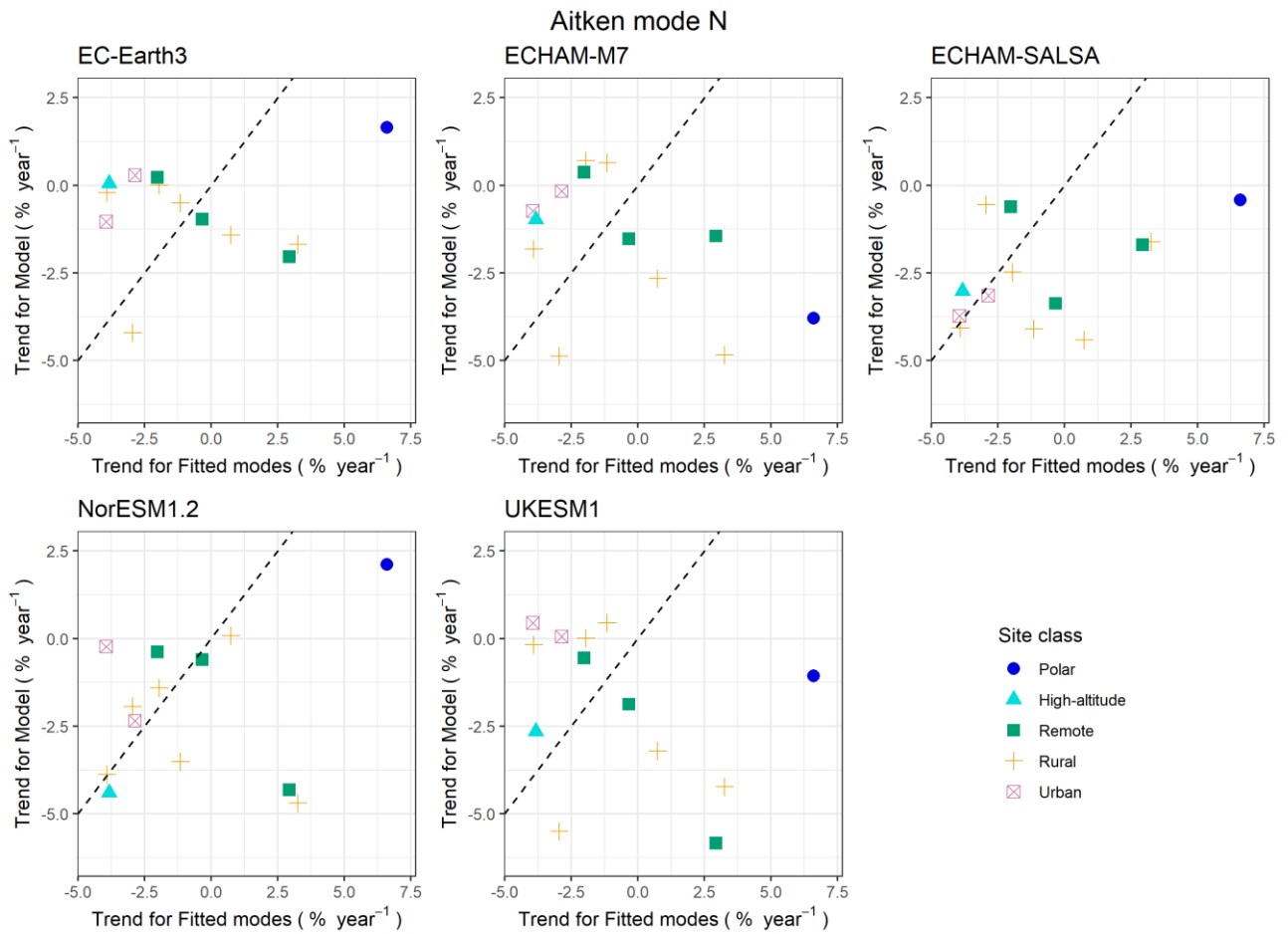


Figure S15 Scatter plots of number concentration (N) long-term trend estimates of measurements (Fitted mode) and climate models (model as a subplot title) for Aitken mode based on the data used for model comparison. Colour and shape of dots represent the site classification of each site (see Table 1 for environmental site classification).

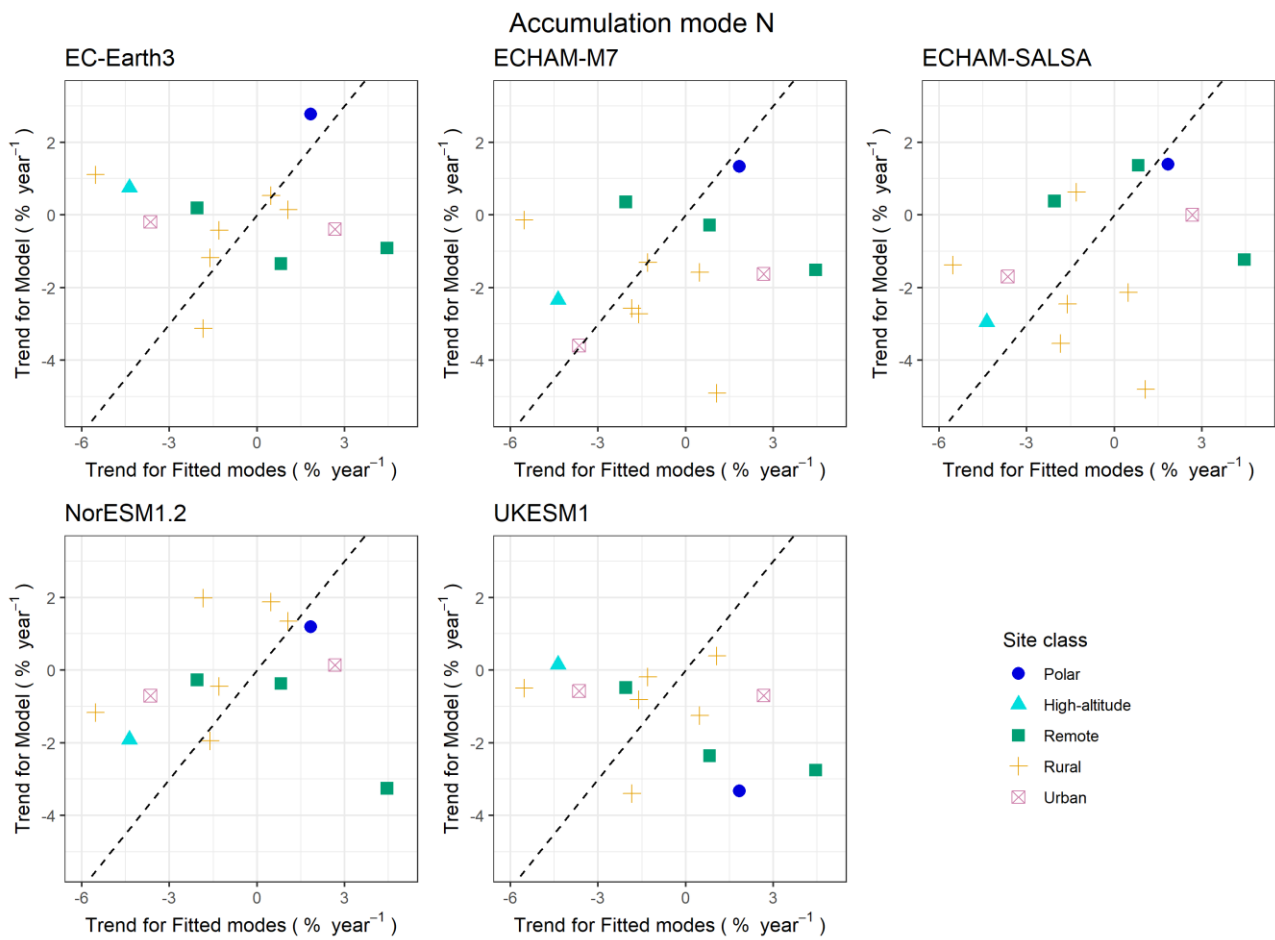


Figure S16 Scatter plots of number concentration (N) long-term trend estimates of measurements (Fitted mode) and climate models (model as a subplot title) for accumulation mode based on the data used for model comparison. Colour and shape of dots represent the site classification of each site (see Table 1 for environmental site classification).

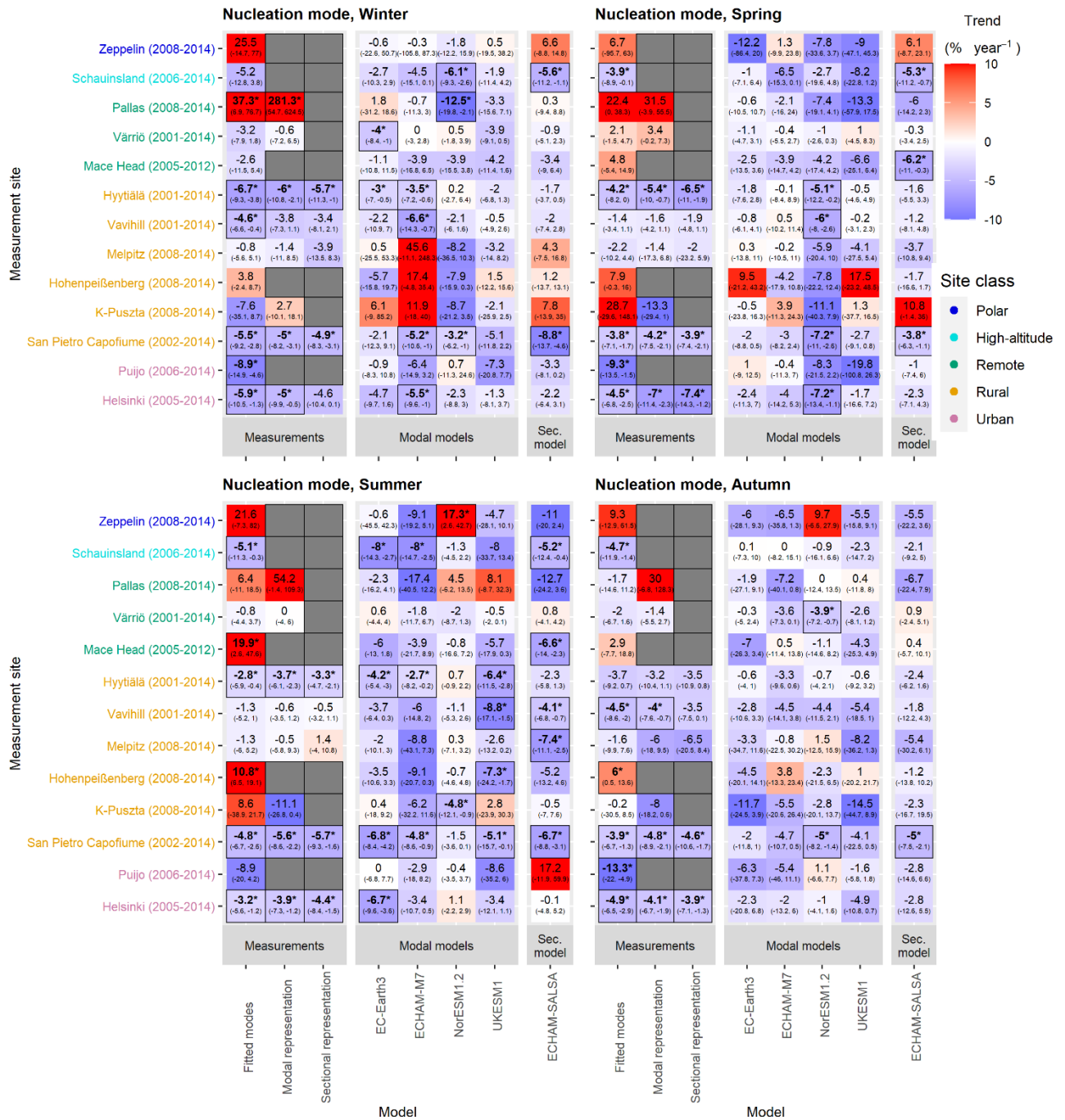


Figure S17 Seasonal trend estimates for nucleation mode number concentration for four seasons: winter (Jan, Feb, Dec), spring (Mar, Apr, May), summer (Jun, Jul, Aug), and autumn (Sep, Oct, Nov). Sites are ordered by site class and within site class from most northerly to most southerly. The bolded number, asterisk, and line border around the estimate indicate that the trend is statistically significant (95% confidence level). Trends have been calculated using Sen-Theil estimator and complemented with bootstrap confidence intervals (see section 2.3.2).

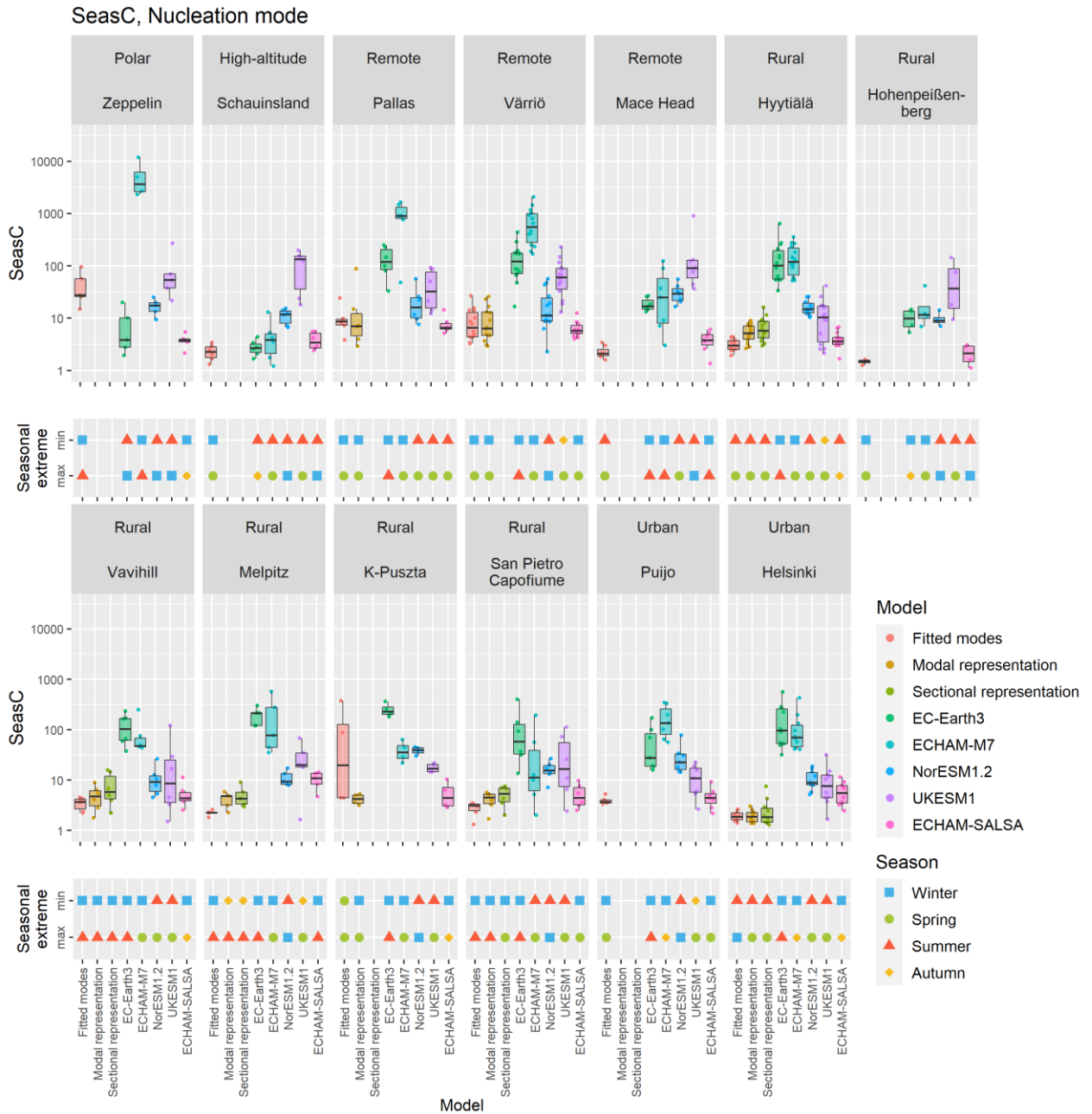


Figure S18 Maximum seasonal variation and seasonal extremes of nucleation mode particles for measurements and climate models. Upper panel: Ratio of maximum and minimum seasonal number concentration (SeasC) for measured and modeled nucleation mode. Points represent SeasC values for single years and box represents the quartiles (1st quartile, median, and 3rd quartile) of SeasC of certain measurement/model in certain site. Whiskers are 1.5*interquartile range. Lower panel: Seasons that most often have had minimum and maximum of number concentrations in measured and modeled nucleation mode.

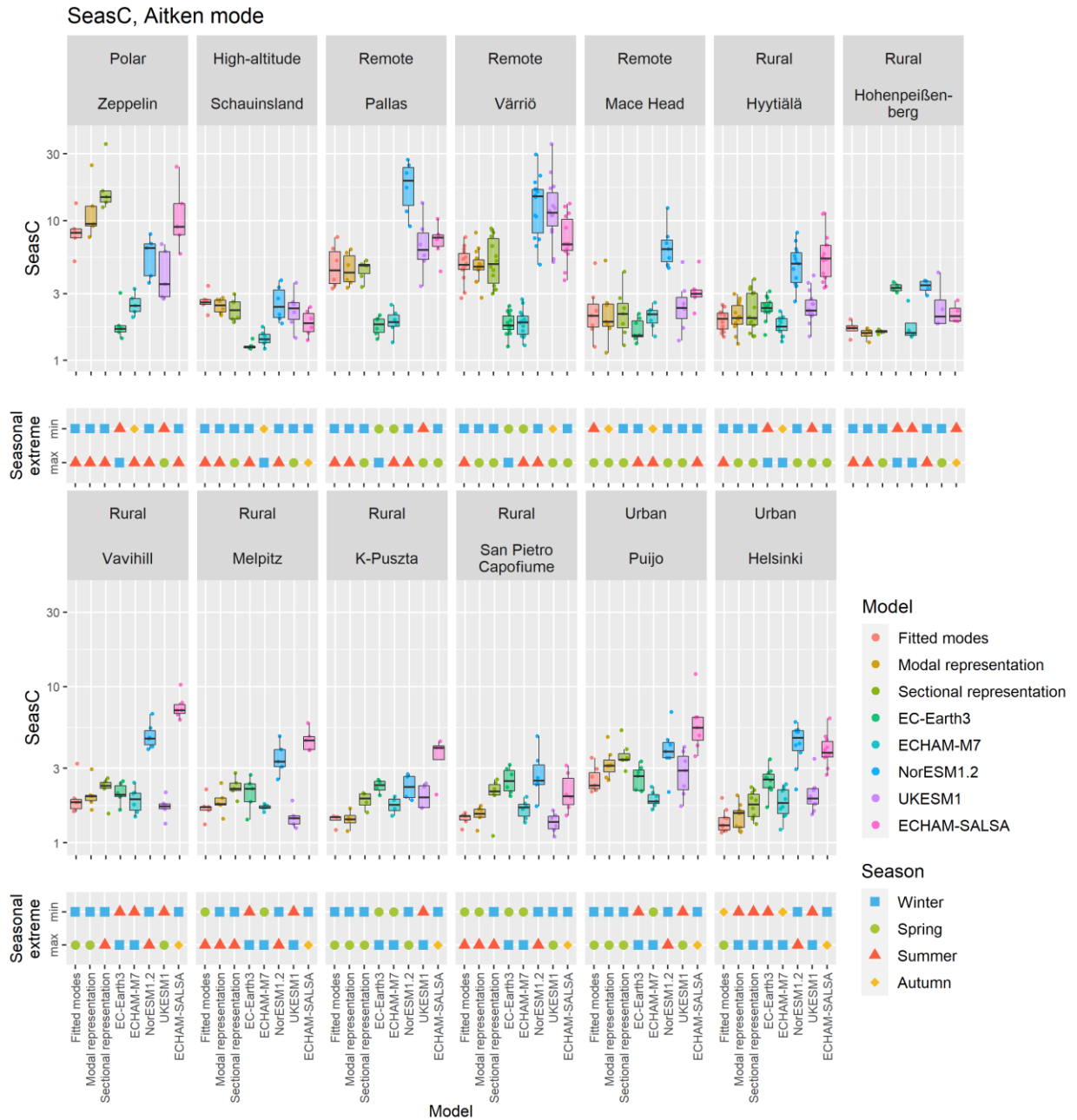


Figure S19. Maximum seasonal variation and seasonal extremes of Aitken mode particles for measurements and climate models. Upper panel: Ratio of maximum and minimum seasonal number concentration (SeasC) for measured and modelled Aitken mode. Points represent SeasC values for single years and box represents the quartiles (1st quartile, median, and 3rd quartile) of SeasC of certain measurement/model in a selected site. Whiskers are 1.5*interquartile range. Lower panel: Seasons that most often have had minimum and maximum number concentrations in measured and modeled Aitken mode.

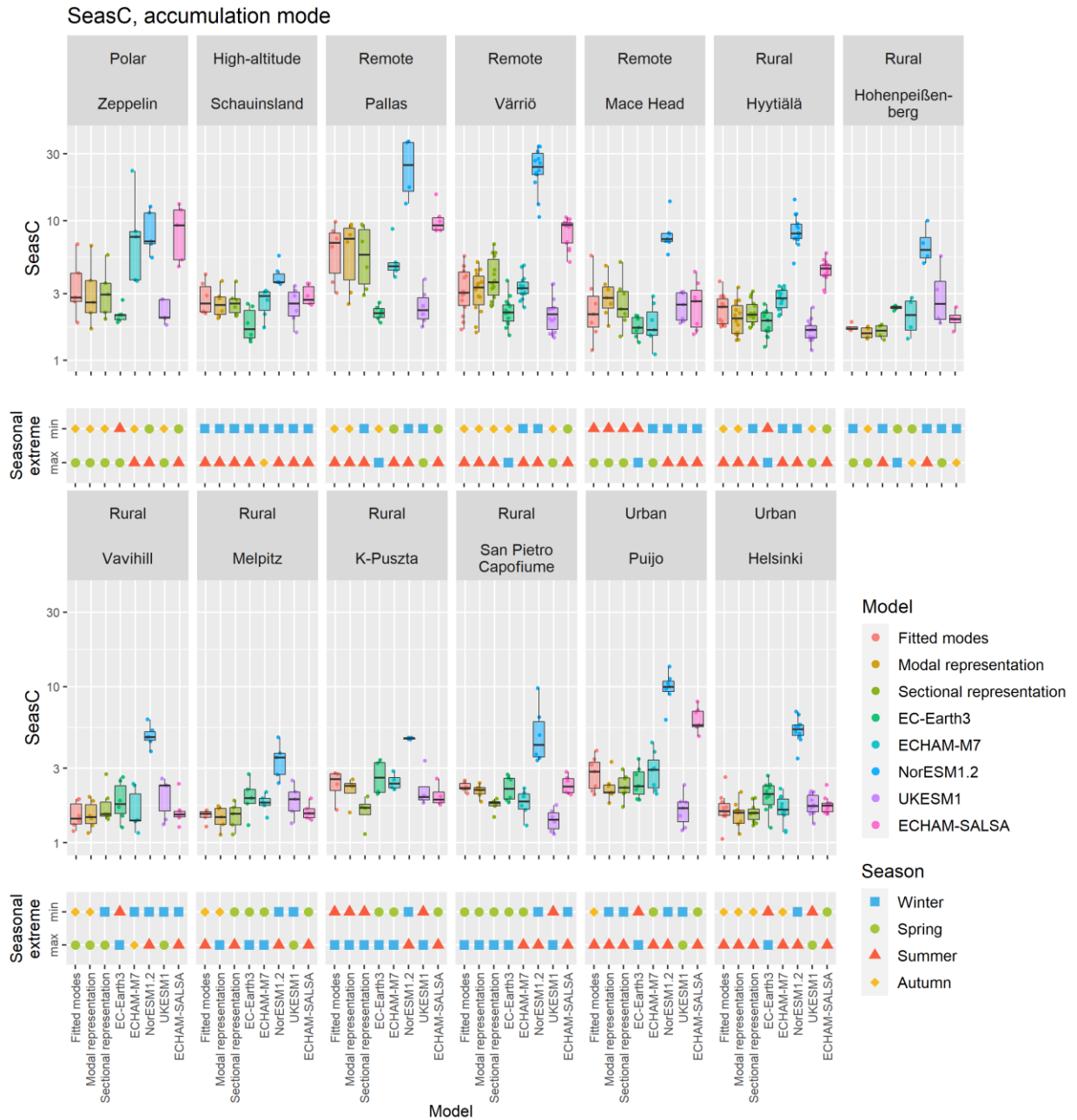


Figure S20. Maximum seasonal variation and seasonal extremes of accumulation mode particles for measurements and climate models. Upper panel: Ratio of maximum and minimum seasonal number concentration (SeasC) for measured and modelled accumulation mode. Points represent SeasC values for single years and box represents the quartiles (1st quartile, median, and 3rd quartile) of SeasC of certain measurement/model in a selected site. Whiskers are 1.5*interquartile range. Lower panel: Seasons that most often have had minimum and maximum number concentrations in measured and modeled accumulation mode.

NIQR, Nucleation mode

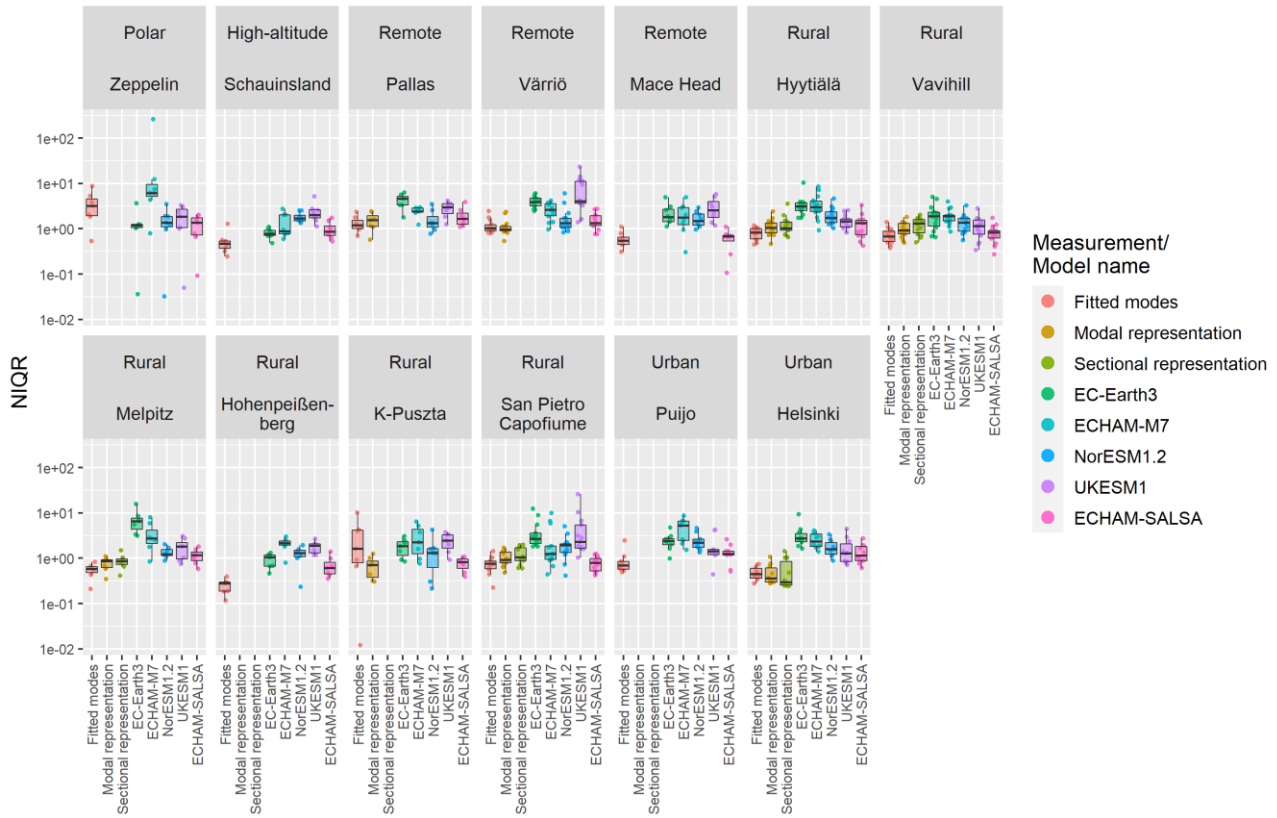


Figure S21 Average seasonal variation and seasonal extremes of nucleation mode particles for measurements and climate models. Normalized Interquartile Range (NIQR) for measured and modeled nucleation mode number concentration in different sites. Points represent NIQR values for single years and box represents the quartiles (1st quartile, median, and 3rd quartile) of NIQR of certain measurement/model in certain site. Whiskers are 1.5*interquartile range.

NIQR, Aitken mode

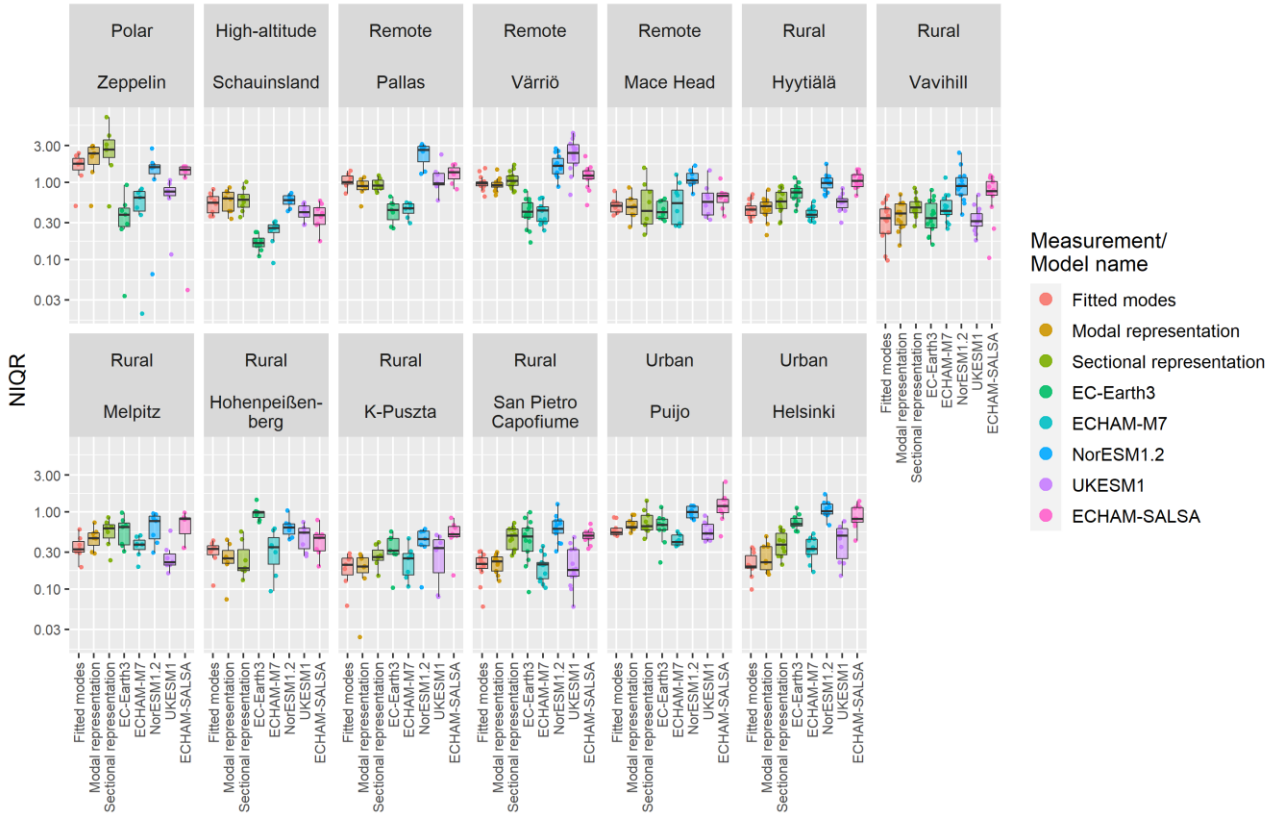


Figure S22 Average seasonal variation and seasonal extremes of Aitken mode particles for measurements and climate models. Normalized Interquartile Range (NIQR) for measured and modeled Aitken mode number concentration in different sites. Points represent NIQR values for single years and box represents the quartiles (1st quartile, median, and 3rd quartile) of NIQR of certain measurement/model in certain site. Whiskers are 1.5*interquartile range.

NIQR, Accumulation mode

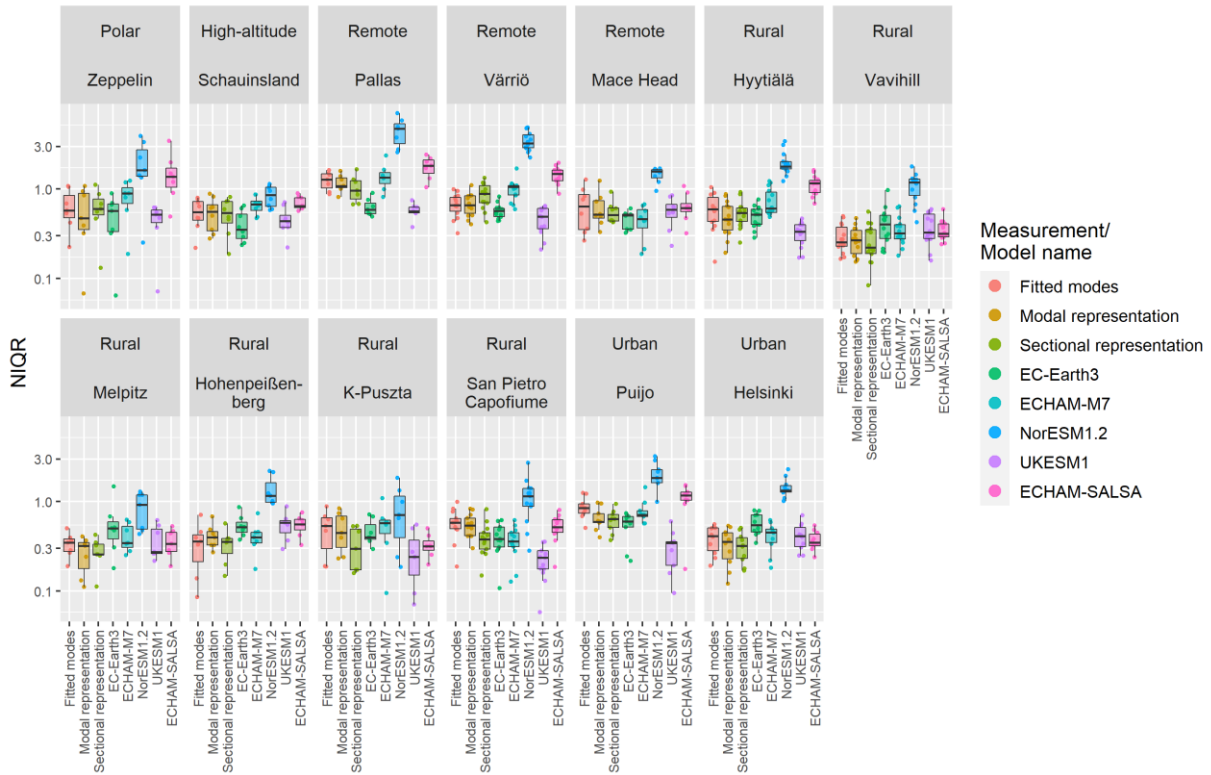


Figure S23 Average seasonal variation and seasonal extremes of accumulation mode particles for measurements and climate models. Normalized Interquartile Range (NIQR) for measured and modeled accumulation mode number concentration in different sites. Points represent NIQR values for single years and box represents the quartiles (1st quartile, median, and 3rd quartile) of NIQR of certain measurement/model in certain site. Whiskers are 1.5*interquartile range.

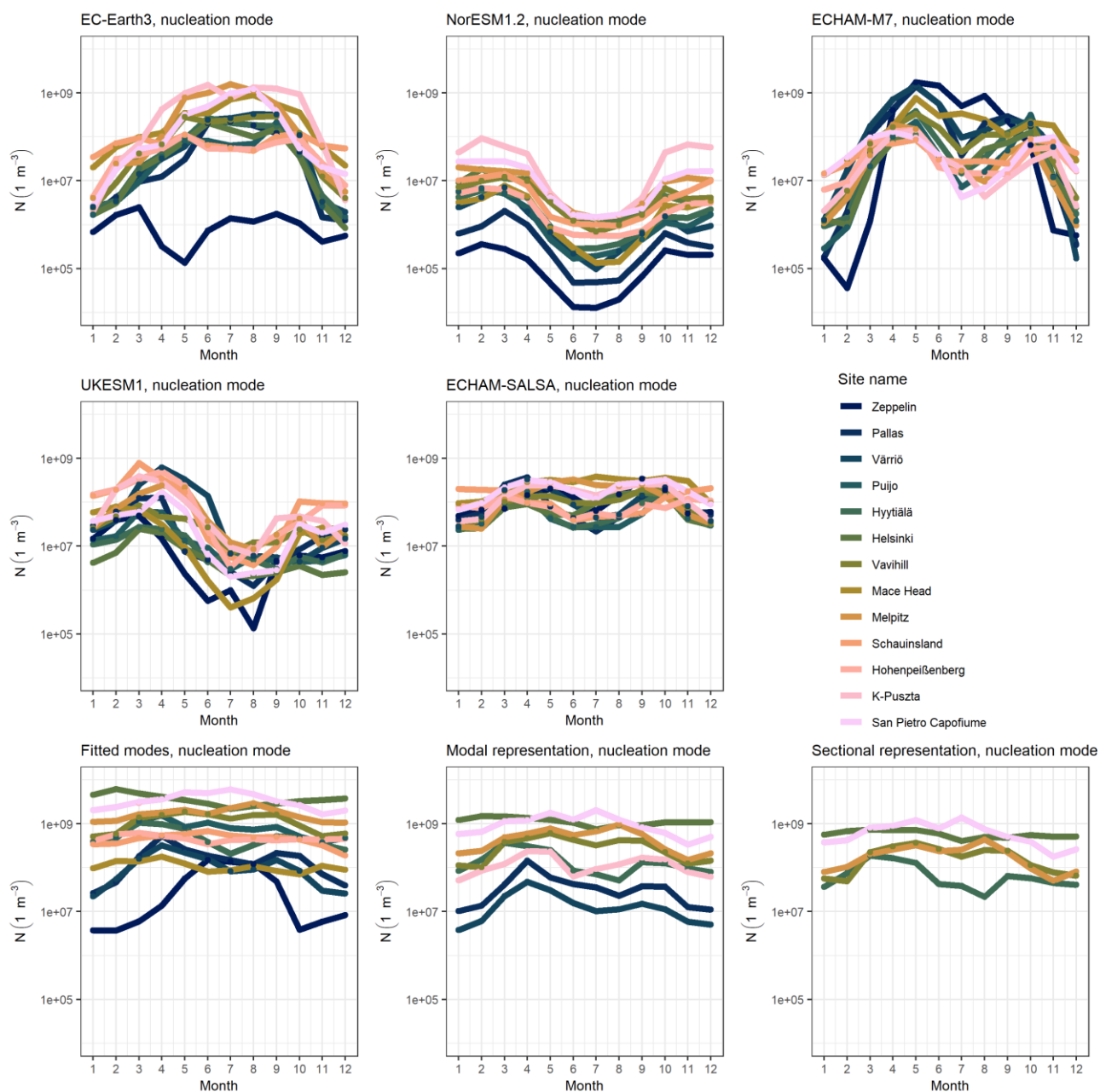


Figure S24 Seasonal cycle of nucleation mode number concentration in measurements and climate models for measurement sites. A subplot represents the seasonal cycle in one model or measurement. Coloured lines represent the median of the monthly means for Aitken mode number concentrations. Sites are ordered from most northerly to most southerly.

References

Rose, C., Collaud Coen, M., Andrews, E., Lin, Y., Bossert, I., Lund Myhre, C., Tuch, T., Wiedensohler, A., Fiebig, M., Aalto, P., Alastuey, A., Alonso-Blanco, E., Andrade, M., Artíñano, B., Arsov, T., Baltensperger, U., Bastian, S., Bath, O., Beukes, J. P., Brem, B. T., Bukowiecki, N., Casquero-Vera, J. A., Conil, S., Eleftheriadis, K., Favez, O., Flentje, H., Gini, M. I., Gómez-Moreno, F. J., Gysel-Beer, M., Hallar, A. G., Kalapov, I., Kalivitis, N., Kasper-Giebl, A., Keywood, M., Kim, J. E., Kim, S.-W., Kristensson, A., Kulmala, M., Lihavainen, H., Lin, N.-H., Lyamani, H., Marinoni, A., Martins Dos Santos, S., Mayol-Bracero, O. L., Meinhardt, F., Merkel, M., Metzger, J.-M., Mihalopoulos, N., Ondracek, J., Pandolfi, M., Pérez, N., Petäjä, T., Petit, J.-E., Picard, D., Pichon, J.-M., Pont, V., Putaud, J.-P., Reisen, F., Sellegri, K.,

Sharma, S., Schauer, G., Sheridan, P., Sherman, J. P., Schwerin, A., Sohmer, R., Sorribas, M., Sun, J., Tulet, P., Vakkari, V., van Zyl, P. G., Velarde, F., Villani, P., Vratolis, S., Wagner, Z., Wang, S.-H., Weinhold, K., Weller, R., Yela, M., Zdimal, V. and Laj, P.: Seasonality of the particle number concentration and size distribution: a global analysis retrieved from the network of Global Atmosphere Watch (GAW) near-surface observatories, *Atmos. Chem. Phys.*, 21(22), 17185–17223, doi:10.5194/acp-21-17185-2021, 2021.